CFD analysis of perforated building geometrical characteristics impact on local wind environment

Anwar E. Hassen

Addis Ababa Institute of Technology

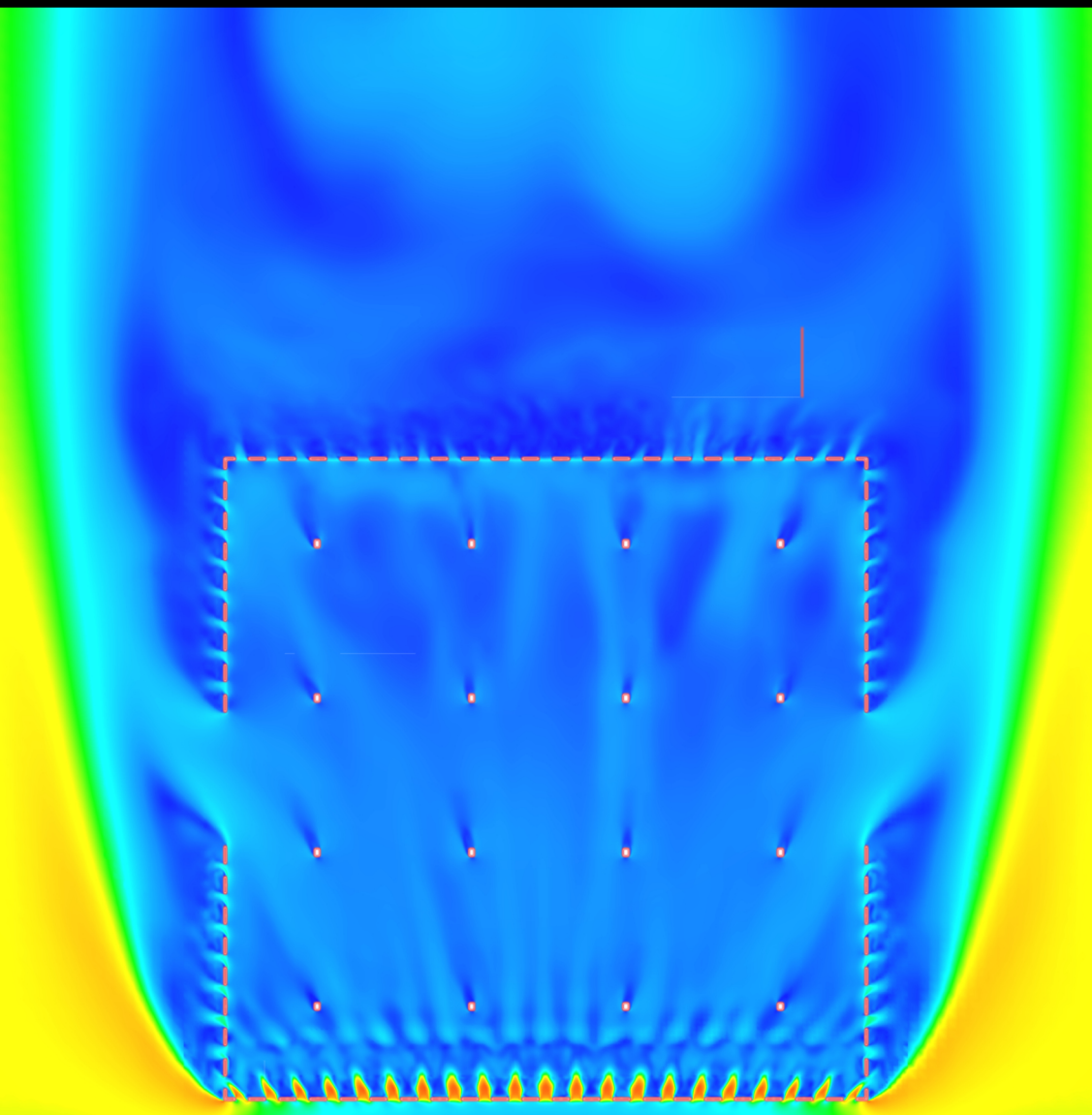

አዲስ አበባ ዩኒቨርሲቲ
ADDIS ABABA UNIVERSITY

CFD analysis of perforated building geometrical characteristics impact on local wind environment

By

Anwar Endris Hassen

in partial fulfillment of the requirements for the degree of

Master of Science

in Mechanical Engineering

at Addis Ababa Institute of Technology

Addis Ababa University

Student ID number: GSR/7513/2013
Supervisor: Dr. ing. Wondwossen Bogale, Assoc Prof.,

An electronic version of this thesis is available at:

June 2022
Addis Ababa, Ethiopia

CANDIDATE'S DECLARATION

I hereby declare that the work which is being presented in the thesis, entitled "CFD analysis of perforated building geometrical characteristics impact on local wind environment", in partial fulfillment of the requirement for the award of the degree of Master of Science in Mechanical Engineering and submitted to Addis Ababa University, Addis Ababa Institute of Technology, School of Mechanical and Industrial Engineering, is an original piece of research work under the guidance of Dr. Wondwossen Bogale, Assoc Prof., to Addis Ababa University, Addis Ababa Institute of technology, school of Mechanical and Industrial Engineering, Addis Ababa, Ethiopia. The matter embodied in this thesis has not been submitted by me for the award of any other degree by any other university or institute.

Anwar Endris Hassen	----------	----------
Name	Signature	Date

ADDIS ABABA UNIVERSITY

ADDIS ABABA INSTITUTE OF TECHNOLOGY
SCHOOL OF MECHANICAL & INDUSTRIAL ENGINEERING

(Thermal and Energy Systems Chair)

CFD analysis of perforated building geometrical characteristics impact on local wind environment

By

Anwar Endris Hassen

Board of Examiners

Dr. ing. Wondwossen B.	_____	_____
Advisor	Signature	Date
Dr. Yilma T.	_____	_____
External Examiner	Signature	Date
Dr. Muaz B.	_____	_____
Internal Examiner	Signature	Date
_____	_____	_____
School Chairman	Signature	Date
_____	_____	_____
School of graduate Studies	Signature	Date

ACKNOWLEDGEMENT

I would like to take this opportunity the express my appreciation for FDRE Ministry of Mines for sponsoring me to undertake this program. I like to thank all my instructors in thermal engineering program. A special granitite of mine goes to my advisor Dr. Ing. Wondwossen Bogale for his continuous guidance that make this project what it is. I would also like to gratefully acknowledge the partnership with SimScale GmbH for sponsoring the tool used in this study. I like to acknowledge Richard Szöke-Schuller, SimScale AEC head, for the continuous technical support throughout the study. And finally, I would like to thank my family and friend for their company.

Abstract

With the need to achieve a net-zero goal in the architectural, construction, and engineering sector, there is a rapid growth in the use of passive building design to reduce buildings' carbon footprint. In this research field, replacing or incorporating ventilation systems with natural means has gained wide popularity across the world. To achieve natural cross ventilation in buildings, building perforation presented as a means of wind infiltration. The design of perforated building façades influenced by different architectural insights including cultural and economic motivations. This led to the introduction of unique geometrical features in urban areas. The literature on potential impact of these geometrical features on the local wind environment is still lacking. Hence, the presented study investigates the effect of geometrical features of building perforation on pedestrian level wind condition under different wind conditions. To achieve that, perforation design from existing building was. A lattice Boltzmann method with a detached eddy version of the K-omega-SST turbulence was model was used to conduct a transient CFD simulation for sensitivity study. The result indicates that different geometrical designs of the perforation can result in different near-faced wind conditions and pressure distribution on the faces despite having the same perforation ratio. The designs also exhibit wind amplification and deceleration effect depending on inflow wind conditions including its speed and direction. Different perforation design parameters have also an impact on the air flow pattern and speed inside the building. Therefore, the result indicates a need to characterize indoor activities for inclusion in comfort criteria and comfort analysis for open space cross-ventilated buildings.

Keywords: Natural ventilation, cross-ventilation, detached-eddy simulation, perforated building, wind comfort, wind speed

Contents

List of Figures

List of Tables

Nomenclature

Abbreviation

ACH	Air change rate (1/h)
AIAA	American Institute of Aeronautics and Astronautics
AIJ	Artictural institute of Japan
AKNKE	Abe-Kondoh-Nagano k-ε turbulence model
AQI	Air quality index (dimensionless)
AT	Air temperature (°C)
BEC	Building energy consumption (W)
BES	Building Energy Simulations
CFD	Computational Fluid Dynamics
CHTC	Convective Heat Transfer Coefficient (W/m2. K)
CKEKE	Chen-Kim Extended k-ε turbulence model
CP	Pressure (coefficient) (dimensionless)
DBT	Dry-bulb temperature (°C)
DKE	Durbin k-ε turbulence model
DNS	Direct Numerical Simulation
DSGS	Deardorff Subgrid-scale
ε (TDR)	Turbulence Dissipation Rate (m2 /s3)
EPMV	Extended PMV (dimensionless)
E (TKE)	Turbulent Kinetic Energy (m2 /s2)
ED	Eddy Diffusivity turbulence model
EBM	Energy Balance Models ECN Economy (currency)
Fr	Froude number (dimensionless)
FYI	First Year Index (year)
HF	Heat flux (w/m2)
HVAC	Heating Ventilation and Cooling
IAT	Indoor air temperature (°C)
k (TKE)	Turbulent Kinetic Energy (m2 /s2)
LRNKE	Low Reynolds Number k-ε turbulence model
LES	Large-Eddy Simulations
LBM	Lattice boatman method
MDKE	Modified k-ε turbulence model

1. Introduction

1.1. Urban Microclimate study background

The United nation's latest report on urbanization indicates 58% of the world population currently live in urban areas and the number expected to grow by 10% within the coming 30 years (United Nations, 2019).With continued urbanization the cover of the built environment with highly populated and denser areas has grown tremendously in the past decades. The built environment aims to provide a comfortable environment for inhabitants. The design and development of urban areas involves consideration of intricate variables to provide convenience for everyday life. Hence, the integration of different urban systems gives the built environment in urban areas unique features all around the world. This understanding of urban areas has emerged a new field of studies that aim to understand the interaction of the built environment with humans in social, economic and environmental aspects.

The necessity of studding urban microclimates is well understood with the scientific community. Hence, the global scientific archive is full of literature to document the accumulated knowledge in the research field. From this knowledge we can understand, despite the position of cities in specified climate zones in the world, the unique features of cities have resulted in a microclimate that is different from the geographical climate (Ai & Mak, 2015; Ampatzidis & Kershaw, 2020; Dissanayaka, 2021; Schinasi et al., 2018). The alternation of climate components such as radiation, wind speed and direction, humidity, temperature, perception etc. due to the built environment has significant impact on inhabitants' comfort and safety (Blocken et al., 2012a, 2012a, 2012b). And as the sole purpose of the built environment, serve inhabitants, the deep understanding of the interaction between urban spaces and inhabitants is important.

In the study of urban microclimate, main findings include, with the rise of global warming and the formation of urban heat islands (UHI), the genuine concern over the effect of heat in human health has shaped the research concentration in the field of thermal comfort in urban environments (Gago et al., 2013). A review of over eleven epidemiological literatures that relate ambient temperature and mortality/morbidity conducted by (Schinasi et al., 2018) find peoples living in hotter parts of the cities have a 6% higher risk of mortality/morbidity. With that in mind, the potential effect of blue and green infrastructures in urban environments to mitigate the formation of UHI has been widely studied in most parts of the world. The other major research area in urban microclimate is the study of Pedestrian Wind Comfort (PWC). The pure mechanical effect of wind has a serious effect on the comfort and safety of inhabitants, shaping how inhabitants live and travel around the cities (Amorim et al., 2014; Blocken & Persoon, 2009; Willemsen & Wisse, 2007a). As a result, numerous criteria and standards have been introduced to manage the problem.

The study of PWC in an urban microclimate requires statistical meteorological data and aerodynamic characteristics of the built environment to attain local wind statistics. Since the Architectural, Engineering and Construction (AEC) community only has control over the aerodynamic characteristics in wind comfort study, the research focuses on understanding the urban features as wind comfort influencing factors. This includes the study of building features effect and building to building interaction. Through the studies, major wind amplification factors such as corner effect, wind down wash effect in high rise building vicinity, passage effects and venturi effects (Reiter, 2010) have been studied extensively.

On the other hand, energy consumption of the urban environment is also another concern in the built environment. As urbanization continues to grow, energy consumption of the built environment also continues to grow. The 2020 global status report for buildings indicates, buildings account 55% electricity end use and contribute 38% total greenhouse emission worldwide (Programme, 2020). To adapt the sector with ambitious international climate change policies, to cut down sector greenhouse footprint and meet a net zero concept, progressive ideas in building design, construction and operation have been introduced. Such efforts have significantly transformed and shaped how we see the environment around us. Arguably one of the major focus areas in the field is the incorporation of passive strategies to utilize nature's synergy to replace some of the most traditional and energy intensive systems in buildings. Of-Course, passive design strategies have been known for a long time, however, the move towards a net zero environment and new digital technological advancement in development of construction techniques, materials, implementations, etc. the scale of passive design strategies further and has grown tremendously in recent years. Such novel approaches have introduced new urban aerodynamic geometrical features that haven't been studied for wind amplification effect before.

1.2. Problem statement

Building HVAC systems account one-fifth of the total building energy consumption, replacing and/or incorporating the system with passive strategy has gained a wide coverage. However, the research in the field mainly concentrated on understanding the extent of energy saving achieved through passive strategies and assisting the effect of passive strategies on indoor thermal comfort (Birol, 2018). Yet the understanding of such systems' impact on pedestrian level wind condition has not been investigated.

Natural ventilation is achieved through two main principles which are buoyancy-driven stack ventilation and wind driven ventilation (Bastide et al., 2007; Brager & de Dear, 2000; Causone, 2016; Chen et al., 2017). In case of buoyancy driven stack ventilation, the cold air enters the indoor environment at low position and as it heats up via heat sources in the indoor environment reducing the density and continues to rise through the building to be ventilated to the outside. Thus, as the air is released at higher height, its effect on outdoor wind comfort is insignificant. Whereas, in wind driven cross ventilation applications the ventilation effect occurs with the presence of pressure difference between the two sides of the buildings (Jiang & Chen, 2002;

Sandberg, 2004; Stavrakakis et al., 2008), and the ventilated air can exist in the outdoor environment at a pedestrian high level. Such cases argue with the authors that it might induce wind comfort effects in the outdoor environment as the ventilated air exits the building. In addition to that, in the case of commercial buildings such as shopping malls, aggressive designs in cross ventilation create significant pressure differences. Thus, the flow of air inside the building could perpetrate a significant mechanical effect to the peoples inside the building creating outdoor like wind sensation.

Figure 1-1. Cross ventilated building (courtesy of Vilalta studio)

Based on the ventilation principle applied, ventilation systems in most cases are provided with a flow control option. For such purposes windows present as the most popular air flow regulation mechanisms. However, recent architectural trend indicates permeable building envelopes are adopted regularly for its high aesthetic value the design gives for streets or open spaces with little or no flow regulation option as shown in Figure 1-1. Beside the pure artistic motivation behind the trend, permeable building envelopes, the designs also have aerodynamic aspects that can influence the wind flow around the vicinity especially when employed to achieve cross ventilation. Since wind permeable building envelope usage has emerged as a new frontier in natural ventilation application, understanding the aerodynamic characteristic has significant importance to provide a proper insight in the planning and design stage of the built environment. To such effort the wind load effect of wind permeable buildings facades has been properly

studied and studies indicate such strategies have a positive effect in reducing a wind load. However, the literature discussing this wind permeable building facade from a PWC perspective is still lacking.

Building facades can be designed with different thickness starting from flat screens, assuming zero thickness. Studies such as (Pool, 2019) have shown that the thickness of the façade has a direct effect on building day lighting and solar shedding performance. However, the literature that studies geometrical and the presence of draft angle in the perforation design in thicker envelopes has not been properly studied.

1.3. Research objective

The presented study will focus on how naturally cross ventilated buildings can affect both indoor and outdoor wind condition. Since there are numerous methods of creating different perforation by using different patterns and different material, the study will only focus on the perforation designs of two dominant designs, square and circular, perforations with a draft angle in a thicker envelope. The expected wind speed effect of the draft angle in such perforation design has motivated the selection of this design for investigation. The study will also investigate the perforation daft angle effect on overall wind comfort in an indoor environment under different wind directions. In addition to that, internal layout and organization of the floor plan effect on overall effectiveness of the cross-ventilation strategy and the wind comfort in both indoor and outdoor environment will be studied. Based on the finding, the study will introduce the need for indoor wind comfort criteria for discussion for intensively naturally ventilated buildings.

General objective

The general research objective of the study aims at characterizing the aerodynamic property of perforated building and investigate the potential impact it has on pedestrian level wind condition.

Specific objective

- Conduct full scale external Wind flow analysis using CFD for comparative models.
- Investigate the potential influence of different perforation design used in natural ventilated buildings over a pedestrian wind condition on both indoor and outdoor environment.
- Map the wind flow patten over the model buildings under different wind condition.

1.4. Significant of the study

As urban environment continues evolve to more complex and integrated structures in coming years, it is essential to properly recognize the impact of different urban features on the inhabitance. This will help our cities to be more equitable for every dweller. As urban climate has a potential to shape people’s everyday life, studding it have a huge benefit on social,

economic and environmental achievement of cities. The AEC industry as showing significant development in recent years; hence, this development introduced some unique features that has not been studied before. Therefore, architects, planners and city developers face the challenge to estimate potential impact on local wind environment. This study aims to contribute to the task updating the current available environmental guideline and building codes through the application CFD analysis to study new urban structures.

1.5. Delimitation

To properly define a parametric relation between perforation design and local wind environment requires an intensive analysis exhaustive parametric combination of different building variables and wind condition. However, since studying all configuration can be out of the timeline set for the current study, the author bound to conduct the study under controlled selection of parameters which includes single perforation ratio, single envelope thickness, two inflow wind speeds, two wind directions, and four geometrical profiles that result in twenty simulations in total.

The current study only focuses on an isolated building with perforations. In an actual urban environment, the aerodynamic interaction between buildings may lead to complexities of wind flow that result in different local wind conditions. Therefore, the likely interaction of a perforated cross-ventilated building with its surrounding building has not been covered.

1.6. Organization of the thesis

The thesis has five chapters. The first chapter, introduction, highlights the main objective of the proposed research and it significant. The second chapter scouts the wide scholarly literature to put into perspective development of wind comfort analysis and energy saving using passive design strategies. As the use of CFD analysis to determine wind comfort in urban areas is significantly high as we can understand from the literature, the first section of chapter three will reflect on the basic numerical derivatives behind the used CFD model. The second section of chapter three discuss over all research design including the development of the case models, parameters configuration, simulation set up and evaluation criteria of the study. In chapter four section one the validity of the proposed model will be investigated using experimental result as a benchmark and the chapter also strive to determine the best mesh development setup for the current research. Following validation section, chapter four discuss the obtained result with the retrospect of other studies. Finally, the last chapter, chapter five, conclude the study with recommendation for further investigation to make the proposed study full.

2. Literature review

The literature review contains three main subtopics. Before we dive deep into the concept and importance of wind analysis in urban areas, it is essential to highlight what parameters of the climate conditions influenced by the development of the build environment and associated changes that emerges for the AEC industries. Thus first, this section will discuss some of the key parameters that changed by urban development and the prospected effect on the human comfort. Second will highlight some of the key passive design strategies adopted in urban development to ensure human comfort and safety.

2.1. Urban climate

The climate in urban areas differs from that in neighboring rural areas, because of urban development. Urbanization changes the form of the landscape and produces changes in an area's air. This include changing some of the key climate conditions including temperature, precipitation, humidity and wind. The rest of this section will discuss how urban development can influence the climate parameters.

2.1.1. Temperature

The local thermal field altered by increased urban land use and habitation, leading to the formation of urban heat islands. An urban heat island occurs when the surface temperature and air concentrated in urban regions rather than in nearby suburban or rural areas (Priya & Senthil, 2021; Tsoka et al., 2020). Solar energy received and produced by solar radiation and anthropogenic activity is divided into three categories: warming the air above the surface via convection, evaporating moisture from the urban surface system, and storing heat in surface materials like buildings and roads. Solar energy normally stored throughout the day and released at night. The bulk of solar energy retained by dark building materials such as impermeable soil, and paved surfaces. Larger heat islands are possible as a result, which enhances thermal discomfort. In metropolitan locations, surface reflectivity has an influence on ambient temperature. It may reach 52 °C when the vegetative surface is dark and dry, but only 18 °C when the land is bright and damp (Dissanayaka, 2021; Ricci et al., 2022).

2.1.2. Precipitation

Because cities are warmer, suffocating air is more likely to ascend, and if humidity levels are high, convectional rainfall — brief, strong bursts of rain and thunderstorms – will result. Dust particles (particularly soot) produced in urban environments, and they function as hygroscopic nuclei, encouraging rain generation (Lenzholzer & Brown, 2016; Motazedian & Leardini, 2012). The city has less snow than the neighboring areas due to the higher temperature.

2.1.3. Humidity

Because cities are hotter, precipitation is unable to penetrate the ground and released into the air by evaporation. Also, transpiration does not occur because cities have less vegetation. Surface runoff often absorbed straight into the subsurface wastewater system and therefore disappears (Ai & Mak, 2015; Bherwani et al., 2020). Because relative humidity is reliant on temperature fluctuations, a better knowledge of urban temperature and water vapor contributions and/or losses would show the causes for decreased relative humidity within cities.

2.1.4. Winds

Because structures function as barriers (wind breaks), wind speeds in cities are frequently lower than in rural areas. However, long roadways with tall and supper tall buildings, on the other hand, can function as wind tunnels, funneling winds down the street and making them gusty as they pass through as shown in Figure 2-1. In addition, the building aerodynamic features have immense influence on how wind condition behave at the vicinity (Jiang & Chen, 2002; Reiter, 2010; Ricci et al., 2022; Willemsen & Wisse, 2007a). This phenomenon has significant impact on pedestrian and determine the purpose of streets, where windy local areas don't recommend for outdoor conditions.

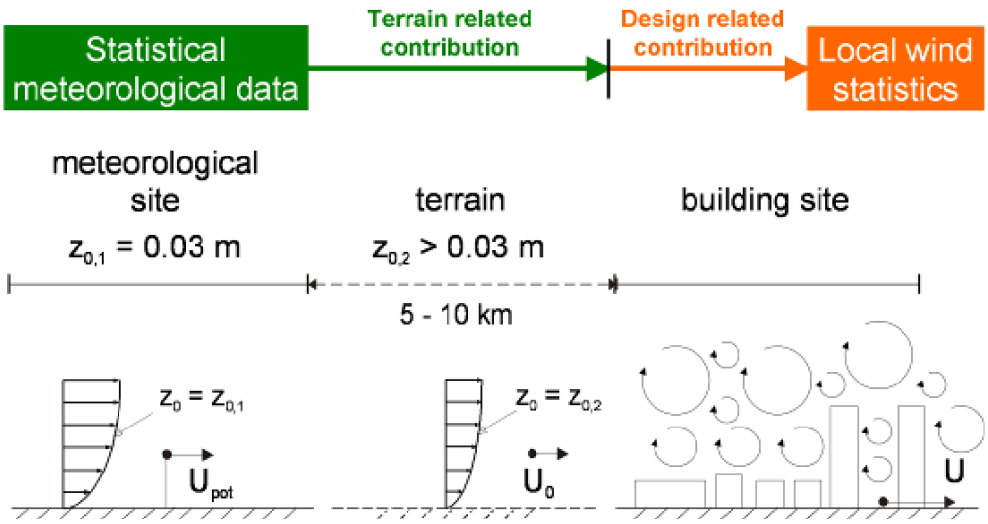

Figure 2-1. The translation of statistical meteorological data from the meteorological site to the construction site is depicted schematically, (Blocken et al., 2012a)

2.2. Human comfort in urban areas

Human comfort in urban environment requires an assessment to make build environment habitable. The major comfort types related to urban climate are thermal comfort and wind comfort.

2.2.1. Thermal comfort

Thermal comfort is the condition of mind that expresses satisfaction with the thermal environment and is assessed by subjective evaluation. The human body can be viewed as a heat engine where food is the input energy. The human body will generate excess heat into the environment, so the body can continue to operate. The heat transfer is proportional to temperature difference (Hami et al., 2019; Yao et al., 2018; Zhang et al., 2010). In cold environments, the body loses more heat to the environment and in hot environments the body does not exert enough heat. Both the hot and cold scenarios lead to discomfort. Maintaining this standard of thermal comfort for occupants of buildings or other enclosures is one of the important goals of HVAC design engineers. Most people will feel comfortable at room temperature, colloquially a range of temperatures around 20-24.5 °C, but this may vary greatly between individuals and depending on factors such as activity level, clothing, and humidity (Aghamolaei et al., 2021; Stavrakakis et al., 2008).

Since there are large variations from person to person in terms of physiological and psychological satisfaction, it is hard to find an optimal temperature for everyone in each space. Laboratory and field data have been collected to define conditions that will be found comfortable for a specified percentage of occupants (Raja et al., 2001). There are six primary factors that directly affect thermal comfort that can be grouped in two categories: personal factors - because they are characteristics of the occupants - and environmental factors - which are conditions of the thermal environment. The former are metabolic rate and clothing level, the latter are air temperature, mean radiant temperature, air speed and humidity. Even if all these factors may vary with time, standards usually refer to a steady state to study thermal comfort, just allowing limited temperature variations. When discussing thermal comfort, there are two main different models that can be used: the static model (PMV/PPD) and the adaptive model.

PMV index uses seven-point thermal sensation scale, which attempts to forecast the mean value of votes cast by a group of inhabitants. When an occupant's internal heat generation and heat loss are equal, thermal equilibrium is reached. Levels of physical activity, garment insulation, and the specifics of the thermal environment may all affect a person's body heat balance. For instance, when occupants of a place have control over interior temperature (i.e., natural ventilation by opening or closing windows), thermal feeling is typically viewed as better. This helps to reduce high occupant thermal expectations on a mechanical ventilation system.

We can anticipate a population's thermal perception using PMV, but this does not provide a complete picture. To acquire a more complete understanding of whether and how thermal comfort may be attained, we also need to take into account the degree of happiness of the space's inhabitants. Fanger created an additional equation to link the PMV to predicted percentage of dissatisfied (PPD).

The PPD, or index, which creates a quantitative forecast of the percentage of thermally unsatisfied occupants (i.e., too hot or cold), can be calculated once the PMV has been established. PPD indicates the proportion of persons who are expected to feel localized pain. Unwanted bodily cooling or heating of a person is the major cause of local discomfort. Drafts, significant vertical temperature changes between the ankles and the head, and/or floor temperature are common causes.

The adaptive model, on the other hand, was created using data from several field investigations with the theory that people interact with their surroundings in a dynamic way. Through their clothes, moveable windows, fans, personal warmers, and sun protection, occupants may regulate their temperature environment. Buildings with air conditioning can use the PMV model, however only structures without mechanical systems can use the adaptive model. There is disagreement about the best comfort model to use for partly air-conditioned buildings that are both geographically and temporally.

2.2.2. Wind comfort

As highlighted in above section wind condition in urban environment is different from surrounding areas. When building aerodynamics characteristics combined with the gusty winds will create a mechanical perpetration that could create unfavorable conditions for urban dwellers (Reiter, 2010). The study of the mechanical wind effect on pedestrian in urban refer as a pedestrian wind comfort. The wind comfort analysis is the combination of statistical meteorological data with building aerodynamic information and comfort criteria. And the importance of the analysis has never been higher as we introduce a unique urban structure in our cities.

Because these unique structures may produce higher wind speeds and stronger gusts at the pedestrian level, wind nuisance, or unpleasant wind conditions, is becoming increasingly essential as an issue to consider for both zoning and construction plans (Janssen et al., 2013; Willemsen & Wisse, 2007b). As a result, it is critical to examine its influence on pedestrians.

Many criteria and regulations exist now to aid in the assessment of the projected wind environment during the design stage, by establishing parameters of what should be done to stay within acceptable limits. From which the Lawson, Davenport, and NEN 8100 wind criteria will be discussed in this section.

These three criteria are deemed comprehensive or full since they include a wide variety of activities, such as "long sitting/standing," "brief sitting," and "strolling." Each of the three criteria has a wind speed threshold value and a maximum permissible exceedance probability of that threshold value.

2.2.2.1. Lawson criteria

The Lawson criteria are determined by the likelihood of a certain place observe wind speeds greater than a specified speed. These speeds are recorded at a certain height, which varies based on the local authority standards but is between 1.5-1.75 meters.

The level of comfort for pedestrians is determined by the varied wind speed threshold settings as well as the probability values. They generally correlate to an action that may be completed in a reasonable amount of time, such as sitting, standing, or quick walking. Statistical meteorological data is used to calculate the likelihood. This information comes from a year-round data collection of wind speed and frequency in 4-36 directions.

Table 2-1. Lawson pedestrian comfort criteria

Wind class	Wind speed	Frequency	Activity
A	> 1.8 m/s	< 2 %	Sitting long
B	>3.6 m/s	< 2 %	Sitting short
C	>5.3 m/s	< 2 %	Walking leisure
D	> 7.6 m/s	< 2 %	Walk fast
E	> 7.6 m/s	>= 2 %	Uncomfortable

2.2.2.2. Davenport Criteria

The Davenport comfort requirements are the most established of the listed criteria and having been published in 1975. This criterion is the first of its type in pedestrian wind comfort standards. For tolerance of wind conditions for activities, the standard sets a maximum exceedance probability of one per week. Although the corresponding exceedance probability is stated to be 1.5 percent, it is unclear how this value was calculated. When comparing Lawson's comfort requirements to Davenport's, one hour each week equals 0.6 percent.

Table 2-2. Davenport comfort criteria

Wind class	Wind speed	Frequency	Activity
A	3.6 m/s	< 1.5 %	Sitting long
B	5.3 m/s	< 1.5 %	Sitting short
C	7.6 m/s	< 1.5 %	Walking leisure
D	9.8 m/s	< 1.5 %	Walk fast
E	9.8 m/s	>= 1.5 %	Uncomfortable
S	15.1 m/s	>= 0.01 %	Dangerous

2.2.2.3. NEN 8100 wind criteria

The Dutch wind nuisance standard (NEN 8100) is the most current of these standards, and it establishes a discomfort threshold of 5 m/s for all sorts of activity. The mean wind velocity of 5m/s is established as the threshold wind velocity for all levels of pedestrian activities in the

NEN 8100 (2006) wind comfort criterion, whereas the mean wind velocity of 15m/s is utilized for the threshold wind velocity of hazard.

Table 2-3. NEN 8100 wind comfort criteria

Wind class	Wind speed	Frequency	Activity
A	5 m/s	< 2.5 %	Sitting long
B	5 m/s	< 5 %	Sitting short
C	5 m/s	< 10 %	Walking leisure
D	5 m/s	< 20 %	Walk fast
E	5 m/s	>= 20 %	Uncomfortable

2.3. Passive design strategies

Many passive solutions exist that use no or very little energy to provide heating, cooling, and lighting for a building through correct design. Because of the high surface area to volume ratio and the lack of internal heat sources in envelope-dominated structures, the environment and surroundings have a stronger impact on the inside of the structure (Rodriguez-Ubinas et al., 2014; Taheri et al., 2021). Internally dominated buildings, such as the conventional office building, are more impacted by interior heat sources such as equipment and people, but the building exterior still plays a critical role, particularly during a power outage. While the line between the two types of buildings can be a bit blurry at times, all structures have a balancing point temperature that is determined by the design and purpose of the structure.

The external temperature at which a structure requires heating is known as the balance point temperature. Because there are more internal heat sources in an internally dominated building, the balance point temperature will be lower, resulting in a longer overheated phase and a shorter underheated period. The balancing point temperature, as well as the interaction with the surrounding environment, play a role in creating a habitable thermal condition during a power outage. Climate-responsive design is an important component of all passive survivability designs. In addition to building function, passive techniques should be adopted based on climate and local factors.

2.3.1. Passive Solar

It is advantageous to be able to passively heat a building during the colder winter months to assist maintain temperature levels. Without the use of mechanical equipment such as fans or pumps, passive solar systems gather and distribute energy from the sun. Passive solar heating uses equator-facing windows (in the northern hemisphere, south-facing glazing) to gather solar energy and thermal mass to store it as shown in Figure 2-2. In direct-gain system permits short-wave solar radiation to enter a room through a window and the solar energy is absorbed by the thermal mass of the floor and walls. And the long-wave radiation is held inside due to the

greenhouse effect as shown in Figure 2-2. To avoid overheating and provide appropriate warmth, proper glazing to thermal mass ratios should be employed.

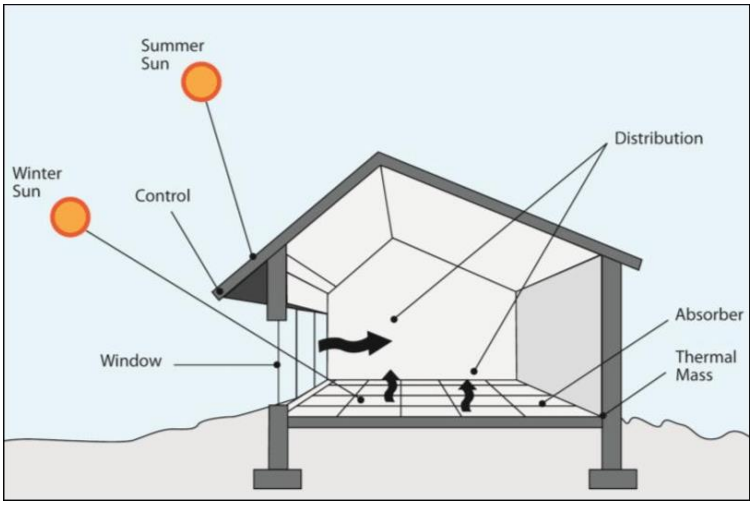

Figure 2-2. Schematic of passive solar utilization design (williams.com, 2018)

2.3.2. Heat Avoidance

During the hotter months of the year, heat avoidance methods can be employed to minimize cooling requirements. This is accomplished using shade devices and the orientation of the structure. In the northern hemisphere, windows should be placed predominantly on southern facades, which get the most sun during the winter, while windows on east and west facades should be avoided owing to shading challenges and strong solar radiation during the summer. Fixed overhangs can be built to block the sun during hot periods while allowing the sun to shine during cool seasons. Because of their capacity to adjust to the environment and the demands of the structure, movable shading devices are ideal. Another excellent approach for reducing heat input is to use light colors on roofs and walls to reflect the sun.

2.3.3. Natural ventilation

Many buildings use an HVAC unit to control their thermal environment. Other buildings are naturally ventilated and do not rely on mechanical systems to provide thermal comfort. Depending on the climate, this can drastically reduce energy consumption. It is sometimes seen as a risk, though, since indoor temperatures can be too extreme if the building is poorly designed. Properly designed, naturally ventilated buildings keep indoor conditions within the range were opening windows and using fans in the summer, and wearing extra clothing in the winter, can keep people thermally comfortable. Some of the designs for occurrence of natural ventilation shown in Figure 2-3.

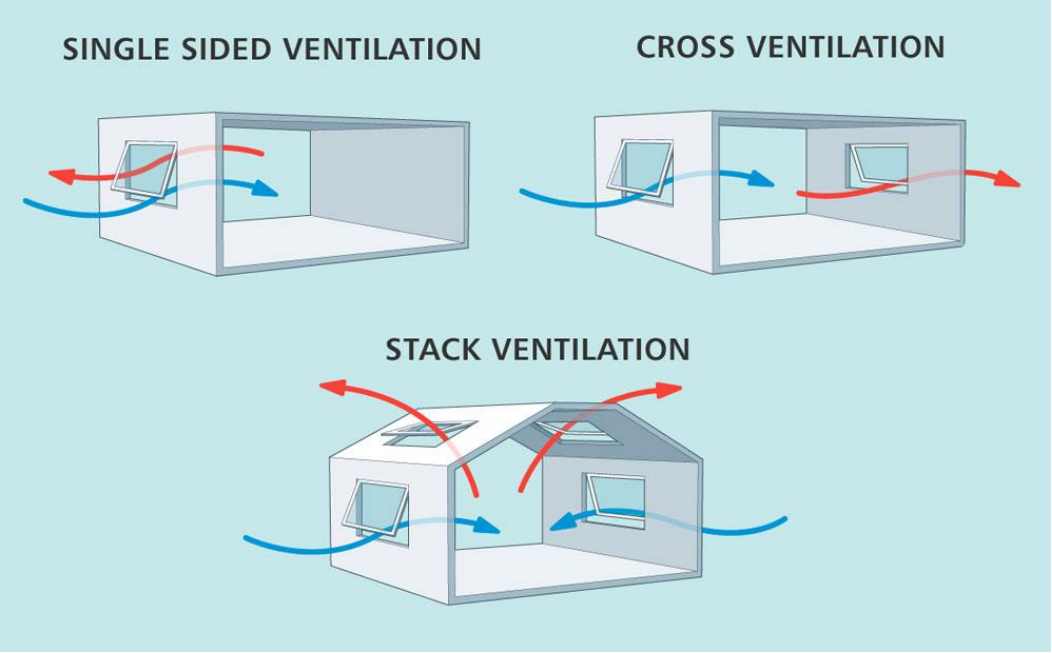

Figure 2-3. Schematic of natural ventilation (rodforctgov.com, 2019)

As shown in Figure 2-3, in single sided ventilation the ventilation process achieved through single air inlet and outlet. Whereas, in cross ventilation, the building is constructed with openings in opposite side of the building where the opening in the windward direction serves as air inlet and the second one serves as outlet. The air movement in cross ventilation achieved through pressure difference in both side of the building. In stack ventilation, the fresh air admitted to the building at lower height and as the air stack up and moves staidly to the upper portion of the building where it provided with chimney structure to let it out to the environment.

2.4. Methods for wind study

To obtain Pedestrian Level Wind (PLW) speed information to assess the local wind environment for wind comfort is mainly conducted by using wind-tunnel measurement and computational fluid dynamics (CFD). In wind-tunnel case wind speed measurement can be conducted using inexpensive technologies such a shot-wire or hot-film anemometer, sand erosion, Irwin probes. Laser-Dropper Atmometer (LDA) can also be used while the cost of such measurement method can be high. CFD PLW assessment can be performed using low-cost Reynolds-Averaged Navier-Stokes (RANS) approach or complex and expensive methods such as Large-Eddy Simulation (LES) and Lattice Boltzmann Method (LBM). This section will review wind-tunnel and CFD use for PLW assessment.

2.4.1. wind-tunnel method

The wind-tunnel measurement approach uses two major instrumentation technics: the point measurement method and the area method. For point speed measurement method employed over

a small area of the domain, measuring instruments such as Hot-wire anemometry (HWA), hot-film anemometry (HFA), pulsed-wire anemometry (PWA), and laser-Doppler anemometry (LDA). While the area measuring method includes scour techniques (such as sand erosion), infrared thermography, and Particle Image Velocimetry (PIV).

Table 2-4. Literature on wind comfort analysis using wind tunnel point method

Author	Instrumentation	Scale	Region	Filed observation
(Kamei & Maruta, 1979)	HWA	Full	Japan	No
(Kawamura et al., 1988)	HWA	Full	Conceptual	No
(Lam, 1992)	HWA	Sized	Conceptual	No
(Murakami et al., 1979)	HWA	Full	Japan	Yes
(White, 1992)	HWA	Full	USA	No
(Blocken, Moonen, et al., 2008; Blocken, Stathopoulos, et al., 2008)	HFA	Sized	Conceptual	No
(Isyumov & Davenport, 1975)	HFA	Full	Conceptual	No
(Jamieson et al., 1992)	HFA	Sized	Conceptual	No
(Murakami et al., 1979)	HFA	Sized	Conceptual	No
(Ratcliff & Peterka, 1990)	HFA	Full	Conceptual	No
(Stathopoulos, 1985)	HFA	Sized	Conceptual	No
(Conan et al., 2012)	LAD	Sized	Conceptual	No
(Sasaki et al., 1997)	LAD	Full	Conceptual	No
(Irwin, 1981)	IP	-	Conceptual	Yes
(Williams & Wardlaw, 1992)	IP	Full	Canada	Yes
(Wu & Stathopoulos, 1994)	IP	-	Conceptual	Yes

The large number of previous studies outlined in Table 2-4 consistently show that the lower-cost techniques HWA, HFA, Irwin probes, and sand erosion produce quantitative results that are very close to those produced by the higher-cost and more accurate techniques LDA and PIV shown in Table 2-5, at least in the so-called "windiest" areas or areas with a high amplification factor. These are the places where determining wind comfort is most critical. Infrared thermography is an exception, where HWA gives different results in the standing vortex.

Table 2-5. Literature on wind comfort analysis using wind tunnel area method

Author	Instrumentation	Scale	Region	Filed observation
(Beranek & van Koten, 1979)	Scour techniques	Full	Conceptual	No
(Durgin, 1992)	Scour techniques	Full	USA	Yes
(Livesey et al., 1990, 1992)	Scour techniques	Sized	Conceptual	No
(Sasaki et al., 1997)	Infrared thermography	Full	Conceptual	No
(Yamada et al., 1996)	Infrared thermography	Sized	Conceptual	No
(Sasaki et al., 1997)	Infrared thermography	Sized	Conceptual	No
(Conan et al., 2012)	PIV	Full	Conceptual	No

2.4.2. CFD method

CFD is receiving growing popularity as a technique for PLW research, as evidenced by a thorough assessment of 50 years of computational wind engineering (Blocken, 2014). This is due in major part to the increasing number of best practice recommendations for CFD that have been published in the previous 15 years, many of which have a special focus on PLW(Blocken, 2015; Blocken et al., 2012a; Blocken & Gualtieri, 2012; Franke et al., 2007; Tominaga et al., 2008). The publication of the new Dutch Wind Nuisance Standard, NEN8100 (Willemsen & Wisse, 2007a), which expressly allows the user to select between wind-tunnel testing and CFD for measuring PLW comfort and safety, has also verified this growing acceptability. When compared to wind tunnel testing, CFD offers certain distinct advantages. It offers data on all essential parameters in all places of the computational domain, known as whole-flow field data.

As a result, CFD can eliminate the two-stage wind-tunnel testing process (first application of area technique followed by application of point technique). Because simulations may be run at full scale, unlike wind tunnel testing, CFD does not suffer from possibly conflicting similarity criteria. This is especially essential in major metropolitan areas where huge scaling factors are required. Parametric studies may easily analyze alternative design configurations using CFD simulations, especially when the various configurations are all a priori embedded inside the same computational domain and grid. The accuracy of CFD, on the other hand, is a source of worry, and verification and validation studies are required.

This issue is also represented in the Dutch Wind Nuisance Standard, which requires quality assurance for both CFD and wind tunnel testing. It's worth noting that quality assurance includes CFD solution testing and validation, as well as thorough reporting of the operation. The approximate versions of the governing equations that are most often employed in wind engineering research are briefly discussed in the following sections

Table 2-6. literature on wind comfort analysis using CFD method

Author	Urban setting	Equation	Key words	Parameters
(Aghamolaei et al., 2021)	Building block	RANS	Outdoor thermal comfort; CFD, Building energy simulation; Tempo-spatial; Surface temperature; Physiological equivalent temperature; Solar radiation	SR, WV
(Amorim et al., 2014)	Street canyon	RANS	--	WV
(Blocken & Persoon, 2009)	Street canyon	RANS	Pedestrian wind environment; Wind conditions; Wind flow; Building; CFD; Numerical simulation; Full-scale experiments; Validation; Sport stadium aerodynamics; Soccer stadium	WV
(Fadl & Karadelis, 2013)	Street canyon	RANS	Computational fluid dynamics, pedestrian wind comfort, built environment and modelling	
(Fallahtafti & Mahdavinejad, 2021)	Building block	RANS	Wind driven natural ventilation, CFD, optimization, window geometry, building aerodynamics, parametric study	WV
(Hu et al., 2018)	Building block	RNG	Wind environment; Residential buildings; Building density; CFD	WV
(W. Janssen et al., 2013)	Street canyon	RANS	Wind nuisance and danger, Airflow, Urban area, Urban aerodynamics, CFD, Built environment	WV
(Kang et al., 2020)	Street canyon	LES	Beaufort wind-force scale, CFD model, Pedestrian wind comfort, Tree drags parameterization, Urban area	WV
(Kang et al., 2017)	Street canyon	LES	CFD model, Tree drags parameterization, Statistical validation, Pedestrian wind comfort, Beaufort wind scale	WV
(Ricci et al., 2022)	Street canyon	RANS	High-rise building, Pedestrian-level wind comfort, Wind-tunnel testing, CFD simulation, Surrounding environment, Vegetation	WV
(Yang & Ye, 2014)	Street canyon	RANS	Residential area, Wall-hanging air conditioning, Thermal comfort, Indoor air quality, CFD simulation	AQ, WV
(Zheng et al., 2021)	Building block	LES	Large-eddy simulation (LES), Façade geometrical details Wind speed, Pressure coefficient' Balcony geometry, High-rise building	

Abbreviations: RANS (Reynolds-averaged Navier–Stokes equations); LES (Large-eddy simulation), RNG (renormalization group), CFD (Computational Fluid Dynamics), SR (Solar radiation), AQ (Air quality), WV (Wind velocity)

3. Approach and method

This section discusses the overall methodology and the research design employed to conduct the study. First the section highlights the numerical approach the CFD model uses. Following that, or pure research reasons and to understand the parametric relation between perforation design and wind condition, the study employs an isolated single building model. Therefore, section 3.2. will discuss the geometrical features of the model buildings. The section also discusses the selected wind speed and direction study.

3.1. A Brief overview of CFD

From the literature review we can understand that CFD become widely popular to investigate urban microclimate specialty local wind climate. This section highlights some of the fundamental principle of the numerical approaches used in current CFD model.

3.1.1. Numerical method

This study employs a Lattice Boltzmann Method (LBM) with a detached eddy version of the K-omega-SST turbulence model to conduct a transient CFD simulation. A commercial GPU-based solver, Pacefish®, developed by Numeric Systems GmbH via SimScale (SimScale, 2022) used in this study. The Lattice Boltzmann method assumes that the macroscopic dynamics of a fluid can be expressed as the collection of the behaviors of all the particles that constitute the fluid. The LBE, which the LBM solves, describes the kinetics of the constituent particles. This equation is derived from the Lattice Gas Automata (LGA), which is constructed as a simplified, fictitious molecular dynamic in which space, time and particle velocities are all discrete. Therefore, particles can only be placed in discrete positions defined by a lattice and move in a discrete manner to the immediate surroundings at each point in time. Note that the exclusion principle remains valid at every timestep and position: no more than one particle is allowed at a given time and node with given velocity. The LBE is the discrete kinetic equation for the particle's distribution function:

$$f_i(x + e_i\Delta x, t + \Delta t) = f_i(x,t) + \Omega i\,(f(x,t)) \qquad i = 0,1,\ldots,M \qquad (1)$$

The number of feasible directions which a particle can move in consecutive time points (i), and consequently their respective velocity direction vectors (e_i), are defined by the lattice dimension and the user preference. Pacefish® uses a standard a D3Q19 scheme, which allows the particles to move in 18 different directions (+ remaining in the cell). Both discrete velocity set and the lattice weights $\{w_i\}$ are expressed in Equation 2 and 3, respectively (Mei et al., 2000).

$$e_i = \begin{cases} (0,0,0) & i = 0; \\ e\,(\pm 1,0,0), e\,(0,\pm 1,0), e\,(0,0,\pm 1) & i = 1;\ 2;\ldots;\ 6; \\ e\,(\pm 1,\pm 1,0), e\,(\pm 1,0,\pm 1), e\,(0,\pm 1,\pm 1) & i = 7;\ 8;\ldots;\ 18; \end{cases} \quad (2)$$

$$w_i = \begin{cases} 2/9, & i = 0; \\ 1/18, & i = 1;\ 2;\ldots;\ 6; \\ 1/36, & i = 7;\ 8;\ldots;\ 18; \end{cases} \quad (3)$$

The evolution between consecutive timesteps is composed by two sub-steps: streaming and collision. The streaming sub-step describes the propagation of the particles to the arrival lattice positions covering the advection of the fluid. Many approaches exist for the collision term ($\Omega_i(n(x,\ t))$), which describes the particle interaction covering the friction of the fluid. One of the most known approaches assumes a linearly stable collision operator, which makes use of a relaxation term known as Bahatnagar-Gross-Krook (BGK). In study (Qian et al., 1992) further developed various models in 3D based on the Lattice Bahatnagar-Gross-Krook (LBGK). Pacefish® offers the LBGK operator as well as proprietary collision operators, which are better in terms of accuracy and robustness. The single-relaxation-time LBGK model is given in Equation 4 (Yu et al., 2003) and the equation updated for collision and streamlining steps in Equation 5 and 6, respectively.

$$f_i(x\ +\ e_i\Delta x, t\ +\ \Delta t) - f_i(x,t) = -\frac{1}{\tau}\left(f_i(x,t) - f_i^{(0)}(x,t)\right) \quad (4)$$

Collision step: $\tilde{f}_i(x,t) = f_i(x,t) - \frac{1}{\tau}\left[f_i(x,t) - f_i^{eq}(x,t)\right]$ (5)

Streaming step: $f_i(x\ +\ e_i\Delta t, t\ +\ \Delta t) = \tilde{f}_i(x,t)$ (6)

Where $f_i(x,t)$ denote particle distribution and $f_i^{(0)}(x,t)$ represents the distribution function at (x,t), τ is single-relaxation-time parameter that controls the rate of approach to equilibrium and e_i is particle velocity along the *i*th direction. And f_i and $\tilde{f}_i$ in equation 5 and 6 denote the pre- and post- collision state of the distribution function, respectively. From the distribution function (Equation (2)), the macroscopic fluid quantities can be derived using the following formulas:

$$Density: \rho = \sum_{i=1}^{M} f_i \tag{7}$$

$$momentum\ flux: \rho u = \sum_{i=1}^{M} f_i e_i \tag{8}$$

The Chapman-Enskog expansion is used to derive the Navier Stokes equations from LBE. In essence, it is a standard multi-scale expansion of the LBE in the nearly incompressible limit. Further details can be found in Viscous flow computations with the method of lattice Boltzmann equation (Yu et al., 2003).

3.1.2. Unit system

To implement this methodology, LBM uses a lattice for the discretization of the fluid as well as an LBM unit system to represent and describe the physical world in the simulation. The choice of the LBM units is based on two factors. First, the simulation should be equivalent to the physical system. Second, the simulation should be sufficiently accurate. Pacefish®, more precisely Pacefish® Backend, uses this unit system for the computation of the simulation. Nonetheless, inside Pacefish® Workbench, two other unit systems coexist with the LBM unit system:

- Dimensionless unit system
- Physical unit system

The mapping between the LBM and the Physical unit system provides the translation of the physical world conditions into the simulation unit space (LBM). The addition of the intermediate unit system dimensionless accelerates the setup of the project. For that reason, that is the main unit system during the setup in Pacefish® Workbench. This unit system must be properly correlated to Physical units to match the simulated real-world setup and it is at the same time mapped to the LBM unit system to control the accuracy and simulation characteristics. The transformation from one system to another is computed by using a Reference Length and a Reference Velocity, which together define the Reference Time.

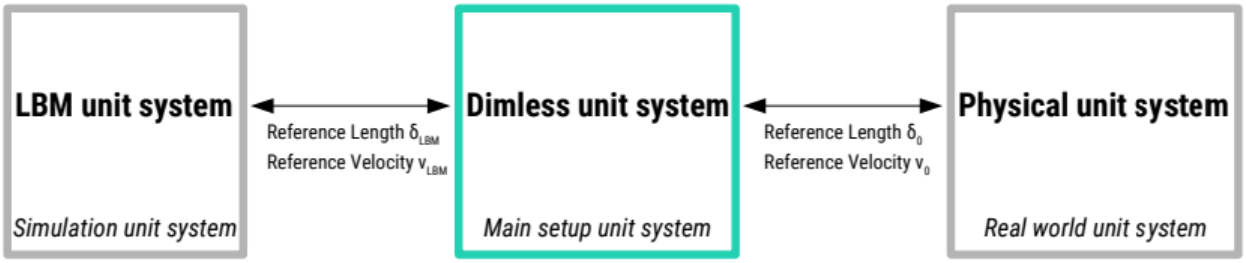

Figure 3-1. Equivalence representation between LBM, dimensionless and physical unit systems

In the background, dimensionless Reference Length (δ_0) and dimensionless Reference Velocity (v_0) are used for the transformation from the dimensionless unit system to the physical unit system. Analogously, LBM Reference Length (δ_{LBM}) and LBM Reference Velocity (v_{LBM}) are used for the transformation from the dimensionless unit system to the LBM system. This mapping is represented in Figure 3-1. This dimensionless scale-independent correspondence between the three-unit systems indicates that they have the same Reynolds number.

3.1.3. Wall Modeling

Close to physical walls, the local properties of a turbulent fluid flow, like the velocity vector, experience strong changes over short distances, resulting in strong local gradients. The Finite Volume Method (FVM)-solvers usually refine the computation mesh to account for the numerical requirements of such strong gradients and local geometrical features. To account for geometrical features, Pacefish® uses sub-grid wall modeling by adjusting the LBM collision distances for particles hitting some inclined or curved wall, as shown in Figure 3-2. To account for numerical requirements, Pacefish® uses a novel proprietary mathematical discretization scheme that allows accurate consideration of strong local gradients. This approach is designed to work around the Cartesian grid related constraints of the LBM, providing high robustness, geometry defect tolerance, and meshing resolution efficiency up to a wall resolution of 2,000 y + units. This unique Pacefish® wall modeling overcomes the need for local "tweaks" of the computation mesh, allowing a fully automated meshing workflow.

3.1.4. Turbulence Modeling

Local fluctuations of the macroscopic velocity vector are called turbulence. The amount of energy contained in this fluctuation is called the Turbulent Kinetic Energy (TKE), k. The turbulent fluctuations usually consist of different lengths and timescales. Large lengths (long-wave) and large timescales (low-frequency) are usually the sources of turbulence. They decay to shorter-scale and higher-frequency fluctuations until the fluctuations become so fine-grained that they dissipate into heat. This is called the Kolmogorov Theory and is depicted in Figure 3-2.

Usually, CFD simulations on an industrial scale are not able to resolve all turbulent scales such that modeling techniques are required to account for the effects caused by turbulence. The most dominant and important effect of turbulent fluctuations on the fluid is the additional mixing contribution.

The Reynolds Averaged Navier Stokes (RANS) (Reynolds-Averaged Navier-Stokes) method incorporates an additional local turbulent viscosity to account for the effects of turbulent fluctuations at all scales, large, medium, and small. This modeling technique is derived by decomposition of the local velocity, pressure, and density into averaged and fluctuating components within the Navier-Stokes equation. The resulting Navier-Stokes formulation can then be simplified to the Navier-Stokes equation of the averaged components, while the fluctuating components are consolidated into an additional stress tensor. This fluctuating stress tensor is then remodeled by the stress tensor of the averaged components as the additional contribution from the artificial Turbulent Viscosity νt. Within this RANS approach, there are multiple models that describe the νt with known variables. From those, Pacefish® offers the KOmegaSST turbulence model. This combines both descriptions of the νt with $k - \omega$ near the walls and $k - \epsilon$ in the far field.

Even though the RANS approach was discovered using Navier-Stokes, the resulting concept of artificial Turbulent Viscosity νt can be applied within the LBM in a similar way. As a result, even though RANS includes the "Navier-Stokes" term, there is no conflict in using RANS turbulence modeling alongside LBM. Because LBM is inherently transient, the unstationary RANS (uRANS) formulation must be used, which allows the turbulent quantities to evolve with time. Separate uRANS turbulence model computes the required turbulent viscosity Vt equations based on the averaged components of the velocity, pressure, and density fields. The value of the turbulent viscosity predicted by a RANS model is independent of the local grid resolution, such that grid convergence studies can be applied.

The Large Eddy Simulation (LES) (Large Eddy Simulation) approach makes use of the ability of the computation grid to resolve large scale turbulent fluctuations, allowing the CFD to represent the dynamics of these fluctuations directly in the local velocity vector and pressure states, making the simulation more accurate in the spatial and temporal sense. Only the finer turbulent fluctuation scales, which are not resolved by the local grid, must be modeled by additional turbulent viscosity. Therefore, the value of the turbulent viscosity t of a LES turbulence model is below that of a RANS turbulence model. Also, this value becomes smaller when the local grid gets finer as a smaller fraction of the turbulent fluctuations must be modeled. Therefore, grid convergence cannot be expected using LES, unless the LES comes very close to Direct Numerical Simulation (DNS), where all turbulent scales are resolved by the local grid.

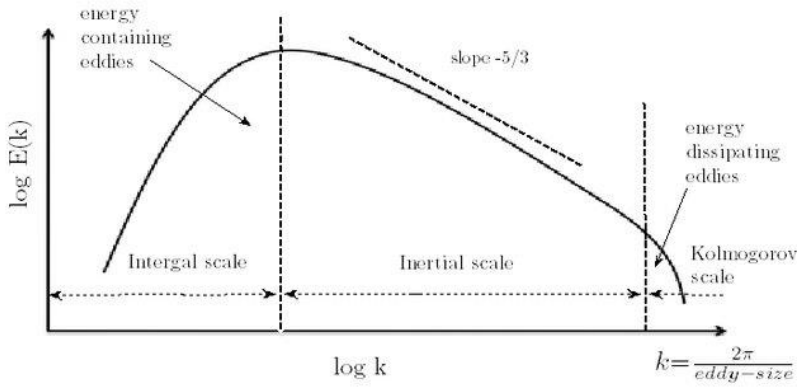

Figure 3-2. Kolmogorov energy transfer theory (Sinha, 2013)

The LES approach works very well in the far field, but to make use of it close to solid walls, a very high wall resolution must be provided on the scale of $y+ \ll 10$, which is not feasible for LBM industrial scale applications. The DES approach is used to overcome this limitation by using hybrid RANS-LES turbulence modeling. Pacefish® provides the SST family's hybrid turbulence models: SST-Delayed Detached Eddy Simulation (DDES) and SST-Improved Delayed Eddy Simulation (IDDES). Close to solid walls, these turbulence models use the uRANS approach, enabling a robust solution for underresolved walls up to $y+ \leq 2,000$. In approaching the far-field, i.e., the free fluid flow, these turbulence models blend over to the LES-approach to resolve the large-scale fluctuations and fluid dynamics directly in the transient velocity vector and pressure states.

3.2. Perforation design

Design indicators that cover environmental, socio-cultural, and economical aspects of the host communities influence the design and patterns of the perforation. Thus, taking this aspect in the design process could result in a different perforation design depending on the host environment. This study focuses on a perforation design in a building featured in BBC Africa iconic architecture 2021 (Ijeoma, 2021), Lideta-Mercato. The perforation design in Lideta-Mercato, shown in Figure 3-3a, follows a simplistic squire design and has a fractal pattern. The area of the perforation increases as it cuts through the skin thickness creating a draft angle. A concrete casting method used to develop the envelope with the designed perforation shape. The presented nozzle-like structure of the building perforation and its expected effect on fluid flow is the main interest area in the current study.

To conduct a sensitivity study on the effect of perforation geometry, the study introduced a circular profile shown in Figure 3-3c with a similar design principle, as the squire model in Figure 3-3b, in the control group. Maintaining a similar wind permeable area is the essential parameter for a model sensitivity study. Thus, the perforation area in both models calculated by equating square and circular area formulas. The model buildings designed with a permeable

area of 200 mm^2. In the modeling process, the inside profile of the perforation profile drawn first on the envelope. The envelope has a thickness of 15 mm and the profile then extruded outward with removal operation at a draft angle. The study also aims to study the potential effect of perforation draft angle on near-faced wind flow. Therefore, the building perforation design have a draft angle of 45° and to help investigate the effect of change in draft angle, a 55° draft angle randomly selected, and a 3D model were prepared.

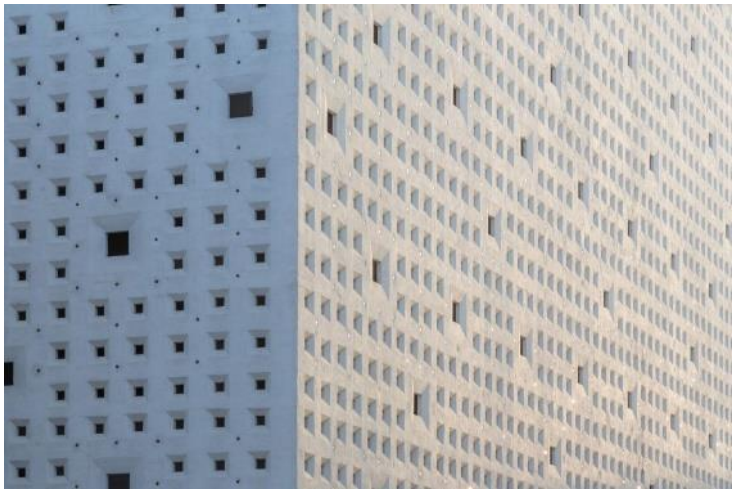

A. Lideta-Mercato Perforation (courtesy of Vilalta studio)

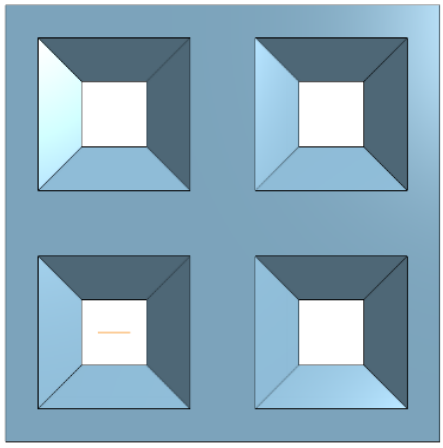

B. CAD model square perforation

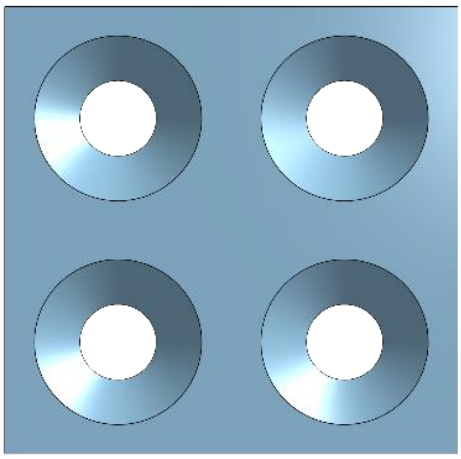

C. CAD model circular perforation

Figure 3-3. perforation design

3.2.1. Case building

A single low rise building with a construction volume of 6.25 $*10^3$ that has the dimension of 25m * 25m * 10m (width (w)* length (L)* Height (H)) selected as a case model. Since the

study aims to investigate the perforated building features amplification effect on wind speed, a full non-perforated building introduced in the model set as a control model. Therefore, the reference model wind amplification effects will serve as a benchmark for perforated models. The general representation of the benchmark model shown in Figure 3-4a. In general, all building models shown in Figure 3-4 contain a cut-through passage that serves as an entry to the building and connects both lateral sides of the building. The building also contains a standard-sized sixteen columns with dimensions of 230mm * 300mm equally separated on the building floor. Since the study interested in building perforation design parameters impact on the local wind environment, the models do not have a floor plan. Only the perforated design taken from the case building, whereas other geometrical parameters discussed in this section do not necessarily describe the case building.

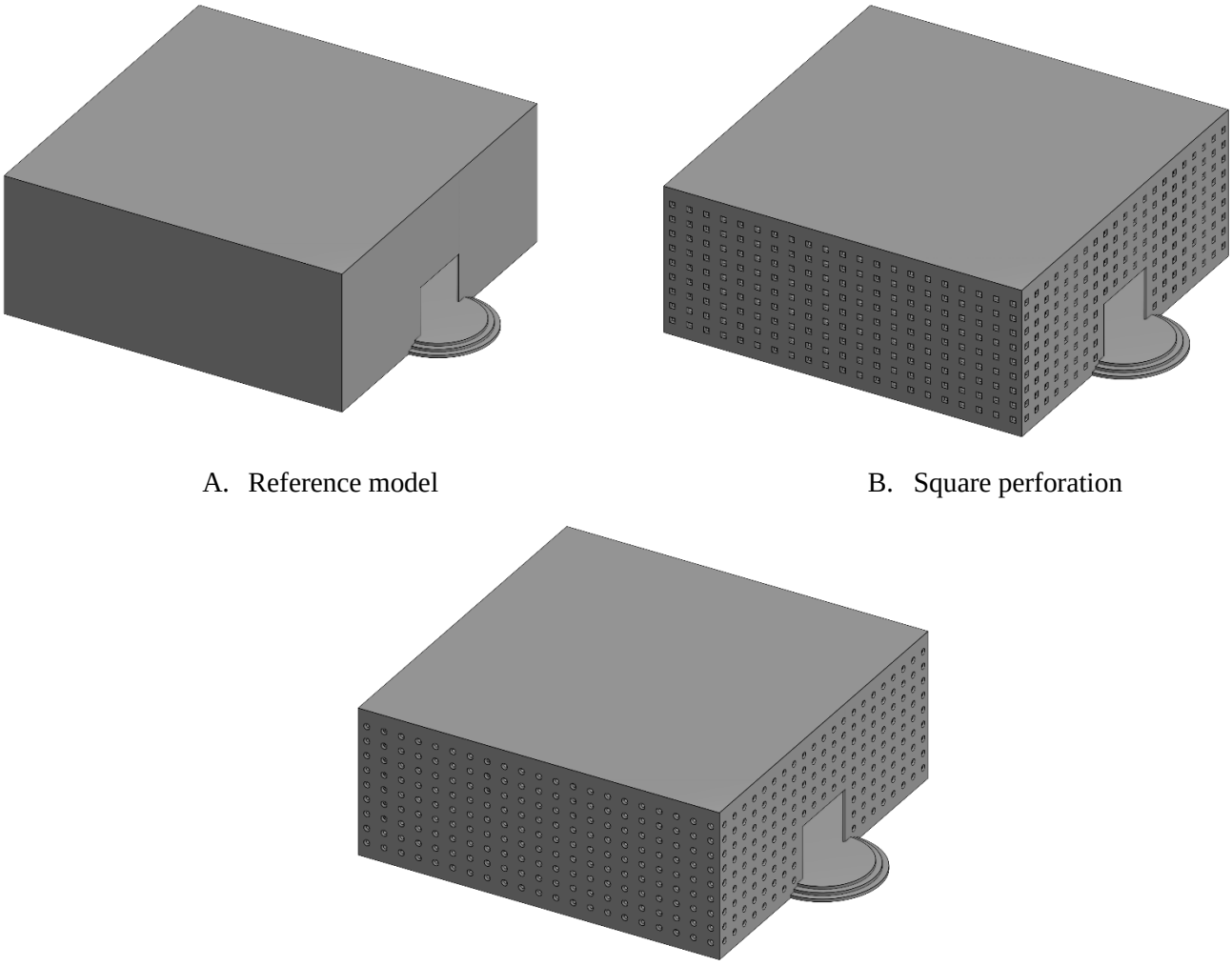

A. Reference model

B. Square perforation

C. Circular perforation

Figure 3-4. Proposed building models

Assessing the pedestrian level wind comfort in both outdoor and indoor of the proposed model is defined by four major factors that include building purpose defining occupants' activities, perforation orientation defining building interaction with wind, perforation pattern and perforation ratio defining the volume of infiltration. In the current study, a single enveloped building proposed for investigation where the perforated layer serves as the boundary of the building separating it from the outdoors. This passive ventilation design strategy gives the building an open-air characteristic. Such open-air designs mostly entertained for shopping malls and recreational centers where activities in the building may include long sitting, standing, strolling, and walking. The perforation considered to be static, always keeping the orientation in place. For natural cross-ventilation application, both the windward and leeward sides of the building faces require perforations. Wind direction varies throughout the year, thus, to ensure effective ventilation all sides of the building faces need to contain perforation on all four building faces. As discussed earlier, two types of perforation design selected for investigation in this study. Therefore, Figure 3-4b modeled with a squire perforation design pattern while Figure 3-4c modeled with a circular perforation. Other dimensional parameters and building features will remain the same with the benchmark model.

The building perforation placement uses an array pattern separated by 1.19m in the horizontal direction and 0.91m length in the vertical direction. With the expected length and height of the building, the building lateral faces hosts 21 perforations and 9 perforations lengthwise and height wise, respectively. The front and the back faces of the building in both perforated building models have a total of 189 perforations. Both lateral sides have door openings in addition to the perforation.

$$Perforation\ ratio = \left\{\frac{PA}{GA}\right\} * 100\% \tag{9}$$

The gross area of the building before peroration (GA) and the area of the perforation (PA) come into a factor to calculate the perforation ratio. Currently, all proposed building models have a building wall area of 250m^2. The front and the back face of the building contain 198 perforations with a single area of 0.2m^2. Therefore, the perforation ratio of each wall calculated using Equation 9 and both perforated building models have a perforation ratio of 14% per wall on the front and backside. The perforation ratio on the lateral side of the building increased by 6% due to the door opening provided.

3.2.2. Wind condition assessment

Winds have dynamic characteristics where wind speed and direction change throughout the seasons. Therefore, assessing wind conditions of urban areas with different combinations of

wind speed and direction is essential to best explore the local wind scenarios. However, since the current study aims to investigate building geometrical features for parametric study, a single wind condition employed instead of wind climate model. Two upper limits of wind speed from Lawson wind comfort criteria, 6m/s and 8m/s, selected for investigation. The study scope allows only single wind speed however the using two wind speed aim cross reference the wind speed effect.

The selection of the two wind speeds motivated by activities in commercial buildings could include leisure and fast walks. In addition to two levels of wind speed, the study also aimed at investigating the inflow of wind from two different wind directions. Therefore, the case building with an approaching wind direction of $\theta=0°$, where the wind direction is perpendicular to the windward façade of the building, and $\theta=45°$ selected. The difference in aerodynamic features of the building in the two directions advised the decision to employ the two wind directions. A total of four wind condition configurations over five building models results in a total of twenty CFD simulations for sensitivity study as shown in Figure 3-5.

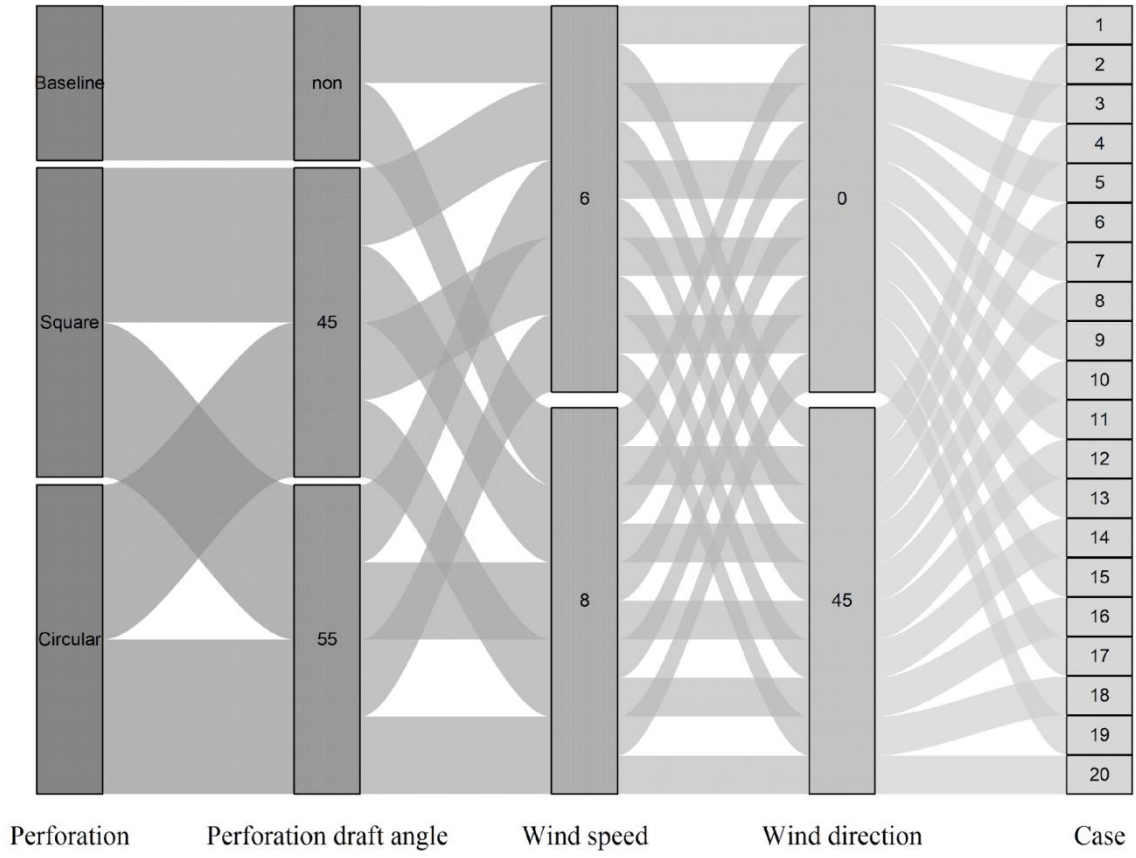

Figure 3-5. Case models parameters combination for CFD analysis

3.2.3. Computational domain

The development of the computational domain (bounding box) follows the best practice guide**.** As discussed earlier the building modeled in full size. In the model buildings, the lateral length of the building is 2.5 times larger than the height. Therefore, instead of using the recommended 5H (where H is the height of the building) length value to establish the lateral and top boundaries, a 2.85% blockage ratio is used to calculate the boundaries without the inclusion of the perforated area in the calculation. The practice guidelines state a length of 5H from the edge of the building to the inlet boundary face would allow the proper development of the wind profile and prevent unwanted streamline gradient in the wind profile. The downstream length seated 15H from the leeward edge of the building.

3.2.4. Boundary condition

To take the effect of the obstacles in urban areas into account, an Atmospheric Boundary Layer (ABL) used to model the inlet wind velocity. ABL consists of the lower region of the atmosphere that influenced by the earth's features and processes (Blocken et al., 2007). With the current application, the developed wind velocity and turbulence intensity are the needed variables. The mean wind velocity (U) profile is logarithmic and calculated using Equation 10 as a function of height (Z). The study uses the reference height of 10m, and a 0.2 aerodynamic roughness length, Z_0, used. K is von Karman constant (= 0.4), the friction velocity U^* value varies for comparative study cases with their respective wind reference velocity, U_{ref}, of 6m/s and 8m/s. The turbulence kinetic energy computed using Equation 11, where C_μ is the turbulence viscosity constant that is equal to 0.09. And finally, since the turbulence model in the study uses the K-omega SST turbulence model for the near the wall condition, the specific dissipation rate (ω) is based on Equation 12.

$$u(z) = \frac{u^*}{K} \cdot \ln\left(\frac{z + z_0}{z_0}\right) \tag{10}$$

$$k(z) = \frac{u^{*2}}{\sqrt{c_\mu}} \tag{11}$$

$$\omega(z) = \frac{u^*}{K\sqrt{c_\mu}} \cdot \frac{1}{z + z_0} \tag{12}$$

The outlet boundary condition is situated as a pressure outlet with a static gauge pressure of 0 Pa. The top boundary condition modeled as a frictionless surface with a slip condition as

shown in Table 3-1. Since the geometry and applied inlet boundary conditions are symmetrical where the two lateral faces are the same size and same orientation with congruent mesh face elements, a periodic or cyclic boundary condition used. Using periodic conditions for the lateral sides will save significant computational time since flux on both faces is the same in magnitude with opposite signs.

Maintaining a proper amount of shear force in the inlet ABL profile requires the definition of corresponding roughness and the value inserted as Sand-Grain equivalent roughness (K_r) in the solver. Since the ABL inlet defined based on aerodynamic roughness (Z_0) in this study as indicated earlier, conversion of Z_0 to K_r required to define the ground boundary condition. Based on the most general relation between K_r and Z_0, Equation 16 in Table 3-1 derived. Using the derived formula K_r value for the current study calculated to be 6.532. Finally, since the solver used in this study optimized for the wind analysis, the building CAD model treated as a non-slip wall condition without user input.

Table 3-1. Boundary conditions

Boundary	Boundary condition	Value	
Inlet	Atmospheric boundary layer inlet	$u(z) = \frac{u^*}{K} \cdot ln\left(\frac{Z+Z_0}{Z_0}\right)$, where $U^* = K \cdot \frac{U_{ref}}{ln\left(\frac{H_{ref}+Z_0}{Z_0}\right)}$	(13)
		$k(z) = \frac{u^{*2}}{\sqrt{C_\mu}}$	(14)
		$\omega(z) = \frac{u^*}{K\sqrt{C_\mu}} \cdot \frac{1}{z+z_0}$	(15)
Outlet	Pressure outlet	Static gauge pressure - 0 Pa	
Top	Slip condition	Normal gradient off all variables - 0	
Lateral sides	Periodic or cyclic condition	Normal gradient off all variables - 0	
Ground	No-slip condition	Surface roughness: $K_r = z_0 * 32.6224271$	(16)

4. Results and Discussion

4.1. Validation and sensitivity analysis

Before to pursue using the software it is essential to conduct robustness test to know the software produces reliable result. The first part of this section employs the Architectural Institute of Japan experimental study to validate the LBM used in this study. On the second section a grid sensitivity analysis conducted to determine the best mesh setup considering result accuracy and computational resource use. From the result the best, mesh development will be identified.

4.1.1. Validation

The Architectural Institute of Japan is a professional association for architects, engineers, and building designers in Japan. It was established in 1886 and now has over 38,000 members. Several periodicals, technical standards for architectural design and construction, and research committee investigations are also published by the organization.

The wind analysis test case for this validation was taken from AIJ's "Guidebook for Practical Applications of CFD to Pedestrian Wind Environment around Buildings", which established standards for cross-comparison of CFD predictions, wind tunnel tests, and field measurements, and helped validate the accuracy of CFD codes for pedestrian wind comfort assessments.

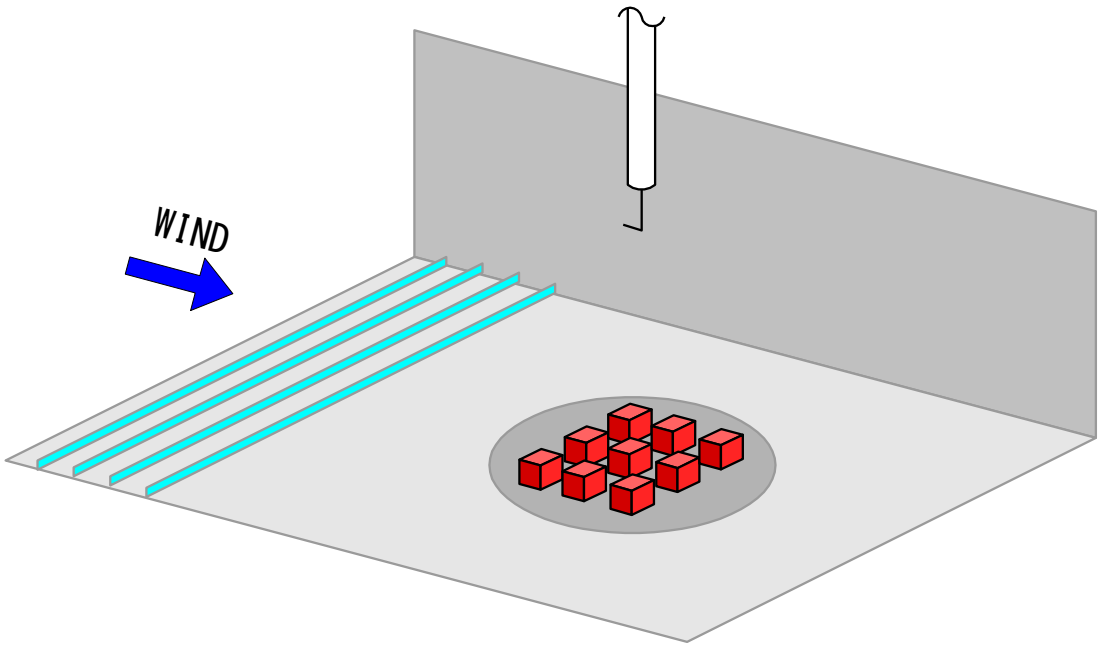

Figure 4-1. AIJ wind tunnel test setup

The goal of this section is to leverage experimental data from the Architectural Institute of Japan to validate SimScale CFD results of Numeric Systems GmbH's LBM approach. Case C is being validated, and AIJ provides experimental data for 9 examples, including 0°, 22.5°, and 45° for three distinct geometries. The geometries depict a tiny block of buildings (see Figure 4-1) with a single entrance.

- No building at the center of middle of the building array
- Low-rise building at the middle of the building array
- High rise building at the middle of the building array

Figure 4-1 the experimental set up the AIJ case c model. All building included in the array form has a cuboid structure where all side of the building measure 0.2m. the wind in flow speed for this analysis at the building height calculated with (UH) was set to 3.65 m/s.

The CAD geometry was created using the geometry data and specifications provided by the AIJ Case C datasheet. The CAD model submitted to SimScale is displayed below, with the main building marked in red and an orange box indicating the position of the measurement points given in Figure 4-2.

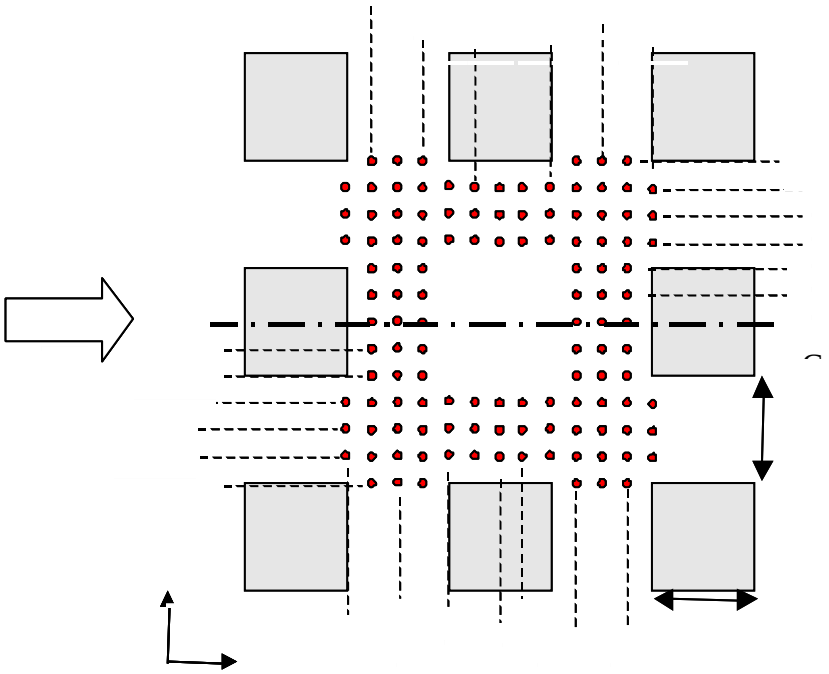

Figure 4-2. AIJ wind analysis probe point position

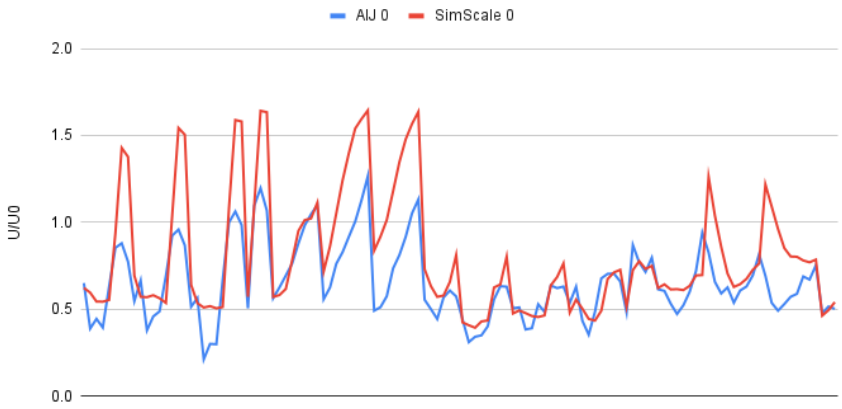

A. For wind direction of $\theta=0^0$

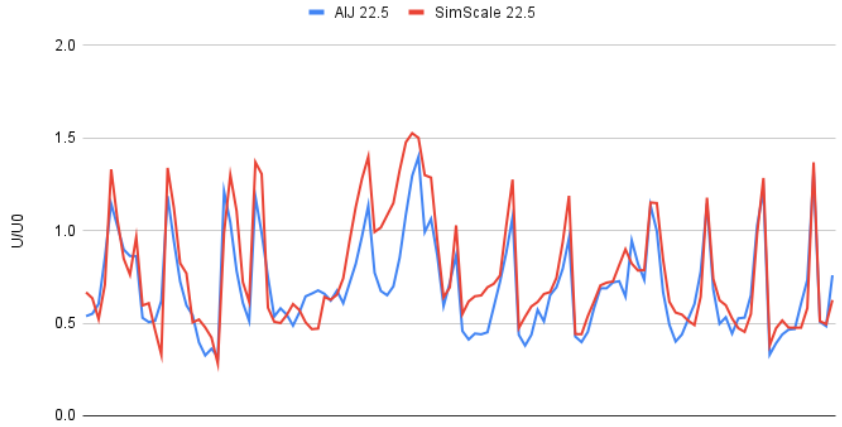

B. For wind direction of $\theta=22.5^0$

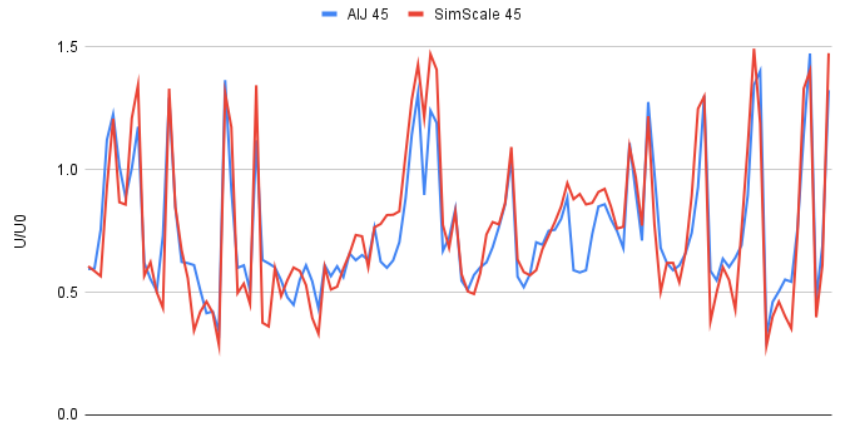

C. For wind direction of $\theta=45^0$

Figure 4-3. SimScale validation with AJI case

This study utilized SimScale's LBM solver for this simulation, which takes a different approach than typical Finite Volume Methods. This solution is based on Numeric Systems

GmbH's Pacefish® and provides several benefits over the old technique, the most important of which are geometry resilience and solver speed in this application. In terms of ABL profiles, Figure 4-2 shows a comparison of the velocity and turbulent kinetic energy (TKE) profiles created by SimScale using the log law with the above-mentioned requirements, as well as the profiles from the AIJ Case C data. The red dashed line in Figure 4-2 depicts the 0.2 m height of the construction components.

Table 4-1. Simulation setup parameters for the case validation model

Solver	Lattice Boltzmann method
Turbulence model	K-omega SST DDES (LES in the far-field with K-omega SST wall modeling)
Wind profile	reference height of 0.2 m, a reference velocity of 3.6m/s and an aerodynamic roughness value of 0.00045 m.
Inlet	Atmospheric boundary layer
Outlet	pressure outlet with a reference pressure of 0 Pa
Ground	no-slip wall without roughness
Side walls of the virtual tunnel	slip wall boundary condition
Size of the tunnel	8 m long x 4 m wide x 1.3 m tall

Maintaining a consistent ABL across the simulation domain is critical for generating a trustworthy result since it assures that the wind conditions operating on the building of interest are the same as the modeler planned. The meshing for an incompressible LBM analysis is based on the lattice Boltzmann technique (LBM), which is distinct from SimScale's finite-volume based fluid dynamics analysis types. A cartesian backdrop mesh is created here, consisting solely of cube parts that are not always aligned with the geometry of the buildings or landscape. There is a sub-grid model that accounts for the interfaces between the geometry and the fluid domains to account for the precise geometry. The mesh has over 82 million 3D cells with minimum cell size of 0.0013m. an automatic refinement on the surface and region refinement on the floor applied for higher mesh resolution. The result of the two cases, AIJ case c dataset and SimScale, plotted in Figure 4-3 and have fair agreement showing the employed CFD method is valid.

4.1.2. Mesh independency test

The size of cells used to discretize the flow domain determines the number of cells and resolution of the mesh. And the result of specific CFD problems highly influenced by the mesh resolution. To make sure the obtained result is not dependent on the mesh size, it is common to conduct a mesh independence test. The study has five geometrical models for investigation under four different wind speed and direction conditions. This configuration takes the needed simulation to twenty. Since conducting the grid independence test on all simulation configurations became computationally expensive, conducting the test on selected one configuration proposed as a viable option. The setting from the test adopted on the remaining

simulation. With that understanding a geometrical model with square perforation selected for the investigation.

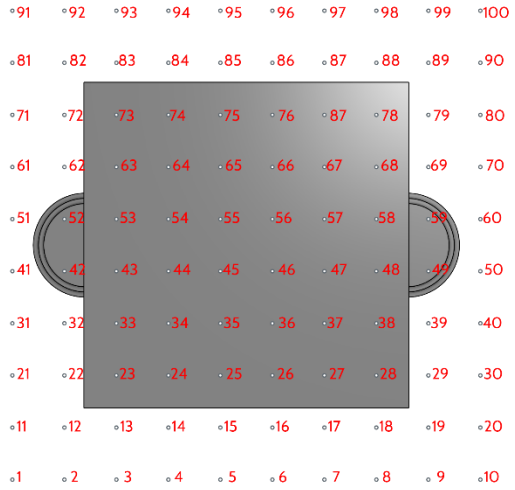

Probe point position

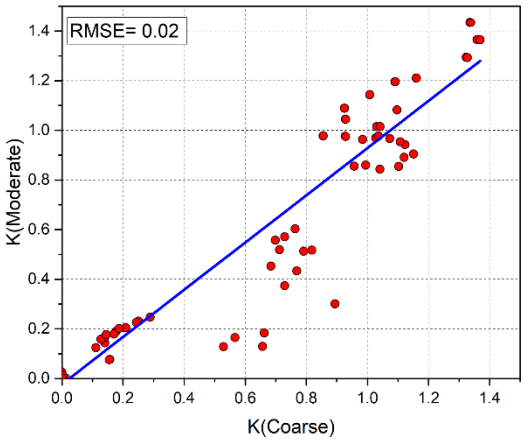

Coarse–Moderate grids

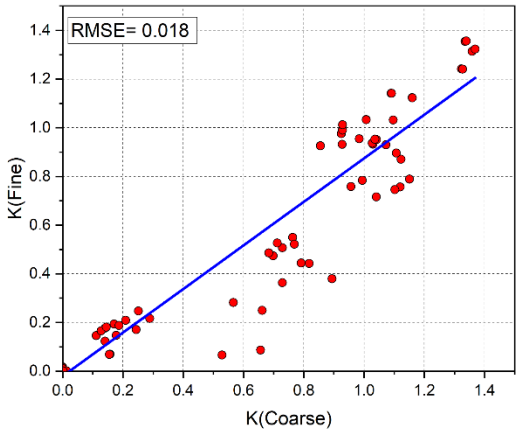

Coarse–Fine grids

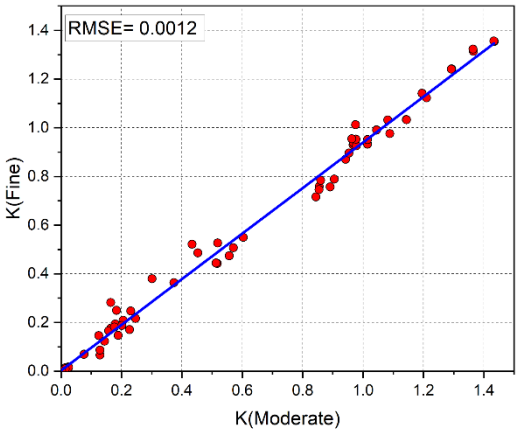

Moderate–Fine grids

Figure 4-4. Mesh dependency test

The study is interested in assessing the building perforation's influence on the wind speed from the pedestrian level. Hence, to help capture the potential effects at the pedestrian level, probe points used for investigation. The test points placed at a two-meter height from the ground and separated by a four-meter distance from each other. The placement of the probe point aims to get sample representation and does not reflect the full scope of the result. In general, the setup led to 100 probe points from which 36 probe points placed inside the building and the remaining placed in the vicinity of the building where pedestrians expected to use. The probe points used to record the variable value of velocity in three directions separately (U_X, U_Y, U_Z)

and the velocity magnitude (U_{mag}), Pressure (P), and Turbulence kinetic energy (K). Since the simulation. transient the record variables have maximum and minimum values throughout the simulation time step. The mesh independent study will use the average turbulence kinetic energy over the time step as a comparison parameter.

Simulation performed using three different mesh sizes with a reference wind speed of 6m/s at a wind direction of 0 toward the windward face of the building. The grid is prepared with an automatic mesh generation option of the solver with coarse, moderate, and fine mesh quality and each mesh has a cell count of over 115, 153, and 271 million, respectively. The solver gradually applied mesh refinements at the near building features, as necessary. The CFD result mesh independency estimated by using the root mean square error (RMSE) of the K value at the proposed data points.

Figure 4-4 presents the comparison of the average k value recorded against a similar variable with a different mesh size. In Figure 4-4b the divergence between coarser and moderate grids is more than 10%, specifically, if the K value is less than 0.8, and led to an RMSE value of 0.02. A slight similar deviation in K observed between coarse and Fine grids in Figure 4-4c with an RMSE value of 0.018. With the final grid combination of K value, moderate and fine grid, a much smaller RMSE value of 0.0012 achieved. A lesser wind speed deviation on the investigation points recorded without significant mesh dependency. Therefore, taking into consideration the computational resources utilized in both moderate and finer mesh resolution to obtain the finding, the study proceeded with a moderate mesh size for the rest of the simulations.

As indicated in section 1, the study is interested in assessing the geometrical effect of building perforation on the local wind environment. To investigate that squire and circular perforation selected for investigation. Thus, this section first highlights the findings on reference models that do not have any perforation. This result will serve as a benchmark to discuss study findings on perforated models in the following section.

4.2. Reference model wind performance

The reference model depicted the most conventional, non-perforated, building. The result presented here represents the wind condition in a horizontal plane at a pedestrian height of 2m where the probe points placed. Figure 4-5 illustrates velocity magnitude color mapped with a wind speed of 6m/s to 8 m/s and b has a wind direction of $\theta = 45°$ with U_{ref} of 6 m/s and 8 m/s wind speed. From visual inspection of the color mapped result, in both wind velocity and direction configuration, the building corners have a wind amplification effect. In $\theta = 0°$ cases, as the reference wind speed increases from 6m/s to 8 m/s the wind separation area also increases. With the presence of the provided door opening the model starts to create wind circulation at the doors when the wind speed increases. Despite these effects, the increment in

reference wind speed has not led to significant wind movement inside the building where both cases show little or no wind movement in the building.

(A)

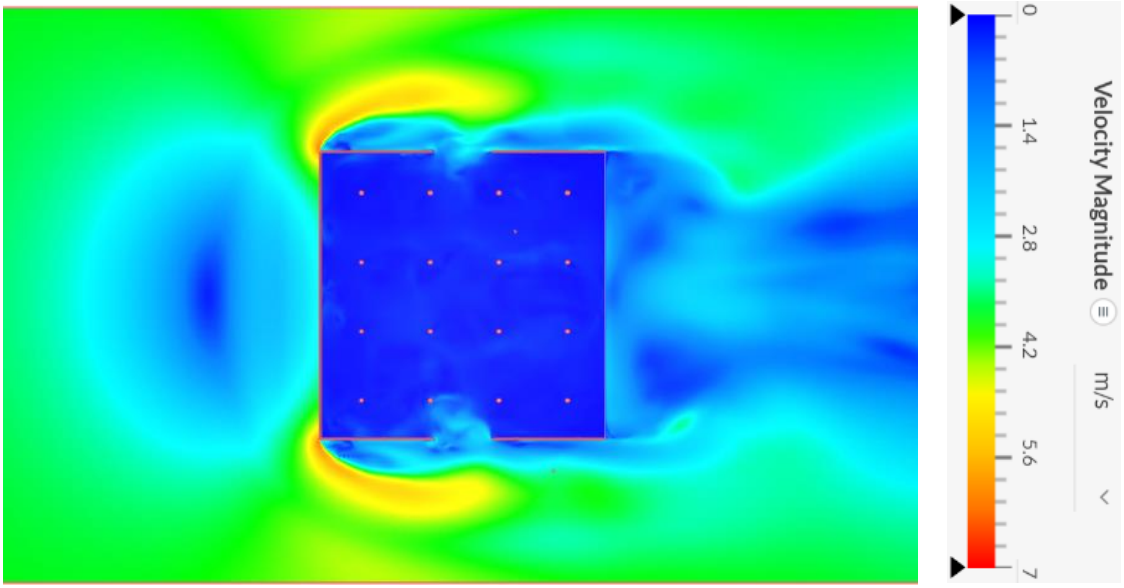

(B)

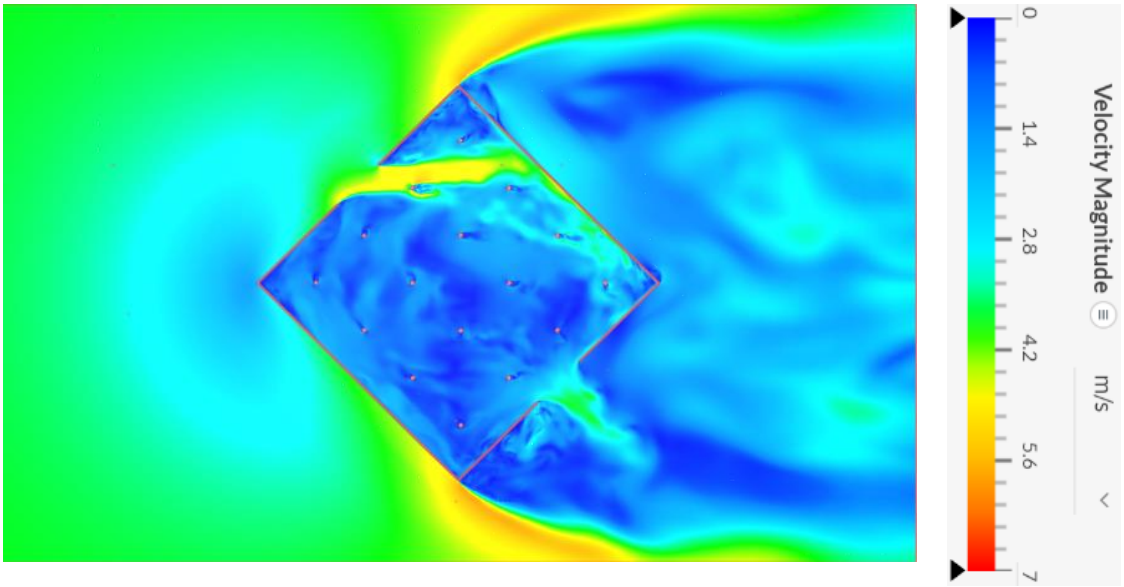

Figure 4-5. Color mapped result of baseline model with 6 m/s wind reference velocity (A) θ = 0° (B) θ = 45°

Whereas in the case θ = 45° has different flow characteristics. The wind direction change causes the model door to become in the windward direction allowing a significant amount of air to enter the building. Since the building faces the wind with the pointing edges of the building corners, the build-up wind pressure in the windward façade significantly decreases. The sharp corner of the building split the wind to the corner edges, thus, more air directed to

the corners recording higher amplification at the edge of the building. The amplification percentage increased by 33% with both wind reference velocities of 6m/s to 8 m/s. The indoor environment of the building presented significant air movement with an average U_{max} of 2m/s recorded at the probe points.

(A)

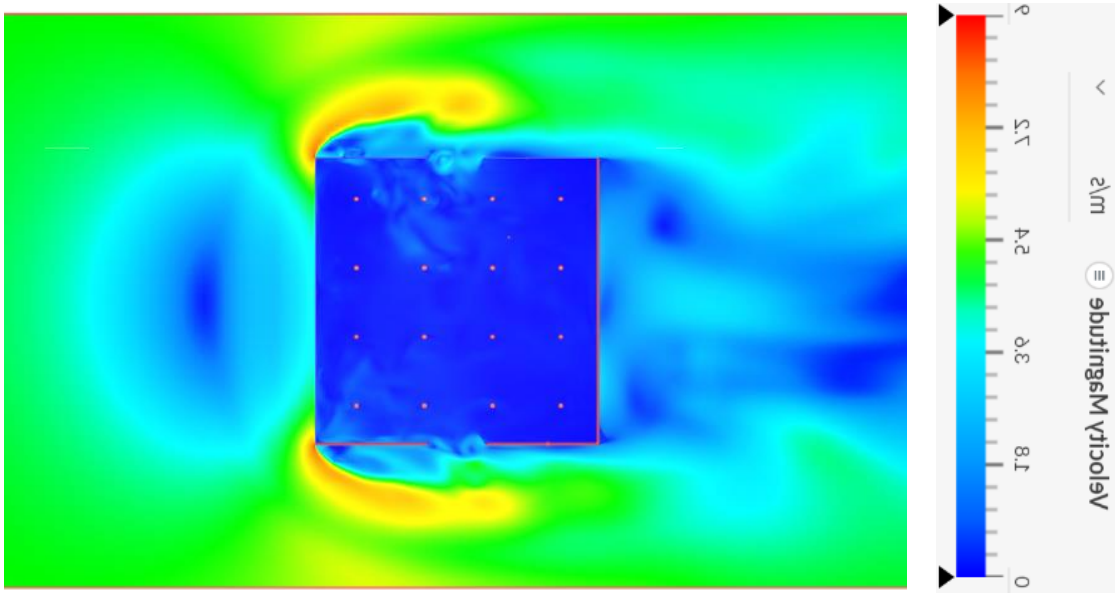

(B)

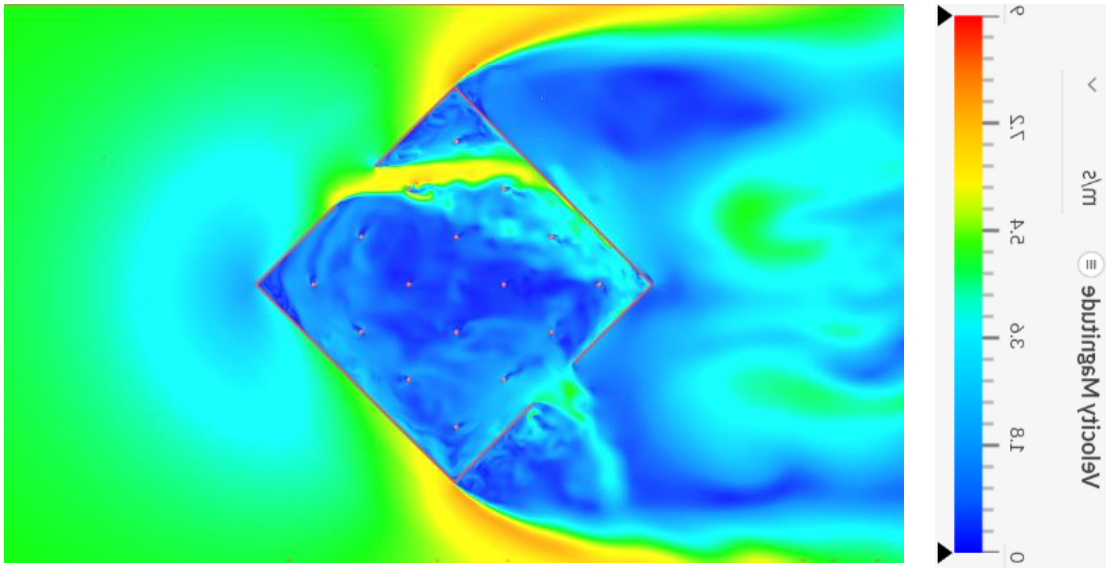

Figure 4-6. color mapped result of baseline model with 8 m/s wind reference velocity (A) θ = 0° (B) θ = 45°

The provided color mapped result in Figure 4-5 and Figure 4-6 can only show as a static wind condition at the final timestep of the simulation that is not a representation of the transient property of the wind. Hence, instead of assessing a color-mapped result at each time step, the study focuses on assessing wind conditions on the proposed measuring points to characterize

wind conditions statistically. As the study focuses on wind comfort, a target parameter of wind velocity magnitude (Umag) is essential to assess comfort level. In this study, the Umag value was recorded over transient conditions on the proposed prob points, and over 400 U_{mag} results were recorded for each probe point. To represent the bulk amount of data, the minimum, maximum and average values of U_{mag} over the transient time become essential statistical parameters.

The statistical parameters can help identify wind exceedance probability and building features wind amplification factor. With the primary review of the dataset, the measuring point positioned inside the building has a significantly lower value than the reference wind velocity. Hence, the dataset starts to skew toward the minimum value when the average U_{mag} calculated. Therefore, to get the pure amplification effect of the building features, the U_{max} value at each probe point considered for the analysis in the rest of the study.

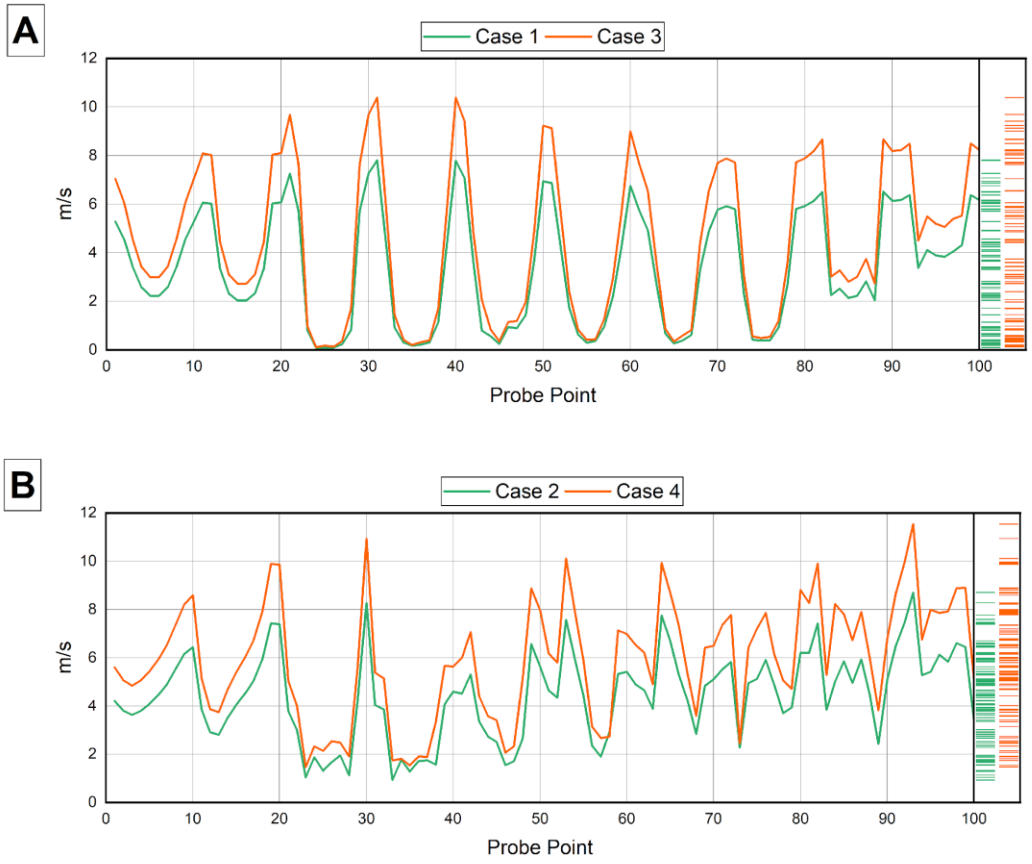

Figure 4-7. Baseline model velocity profile at the probe points

Figure 4-7 plots the U_{max} value of each probe point of the reference cases. In Figure 4-7a cases 1 and 3 U_{max} value presented where both cases have similar wind directions but different wind reference speeds. The U_{max} plot of both cases has similar profiles with just an amplitude difference that resulted from different inlet wind speeds indicating the flow remains similar

despite the velocity increment. In Figure 4-7b, despite the velocity profile maintaining similarity in the first half part of the plot, the graph starts to deviate in the remaining part. This may result from a large part of the building's exposure to the incoming wind including the indoor environment introducing complicated building shapes in creating a turbulence flow. This is not the case for wind direction of θ = 0° as the windward façade of the building remains the major side to interact with the wind and there is little flow inside the building. In both cases, 1 and 3, the highest U_{max} value recorded at the measuring point of 31 with a value of 7.81 m/s and 10.39m/s, respectively. In the case of 2 and 4 probe points 93 records the highest value of 8.7m/s and 11.54 m/s, respectively.

$$v \approx v_{ref} \cdot \frac{ln\left(\frac{z}{z_0}\right)}{ln\left(\frac{v_{ref}}{z_0}\right)} \tag{17}$$

As established in the earlier section, the study uses a roughness length in the wind direction to define the wind velocity at different heights of the computational domain. Since the study is interested in assessing the wind condition at a pedestrian level of 2 m height, the reference wind velocity value at a height of 2 m used as a reference wind speed to calculate the wind amplification factor. Thus, to attain the approximate wind speed at a pedestrian height, the wind velocity extrapolated using the Log law in Equation 6. Using the equation, the wind velocity at pedestrian height approximated 3.5 m/s and 4.7 m/s for the study of two wind reference values of 6m/s and 8 m/s, respectively.

The amplification factor obtained in percentage by calculating the difference between the U_{max} value and the reference wind inlet value at a pedestrian high. This analysis will help to identify a high wind amplification space of the building where the probe point is situated. In the case of wind at a direction of θ = 0°, Figure 4-8a, the wind amplification factor matched between the two wind speeds with only significant deviation recorded only at two probe points. Of the total measurement points, 45 points show an amplification factor, and the remaining 65% show speed deceleration. A higher amplification factor of 1 and above recorded at 6 measuring points near the upstream building corners.

Whereas in the case of θ = 45°, Figure 4-8b, there is a significant discrepancy in the calculated amplification factor between the two cases. In total, cases 2 and 4 recorded an amplification effect in 72% of the measuring points and the remaining have a deceleration effect. This is a 20% present higher amplification effect recorded from θ = 0°. This is the result of more exposure of the measuring point, including probe points inside the building, to the upstream wind as the wind changes its course. The interesting finding from this analysis is that in both

wind directions the amplification factor dropped by 0.32% in θ = 0° and 0.25% in θ = 45° on average when the wind velocity increased from 6m/s to 8m/s.

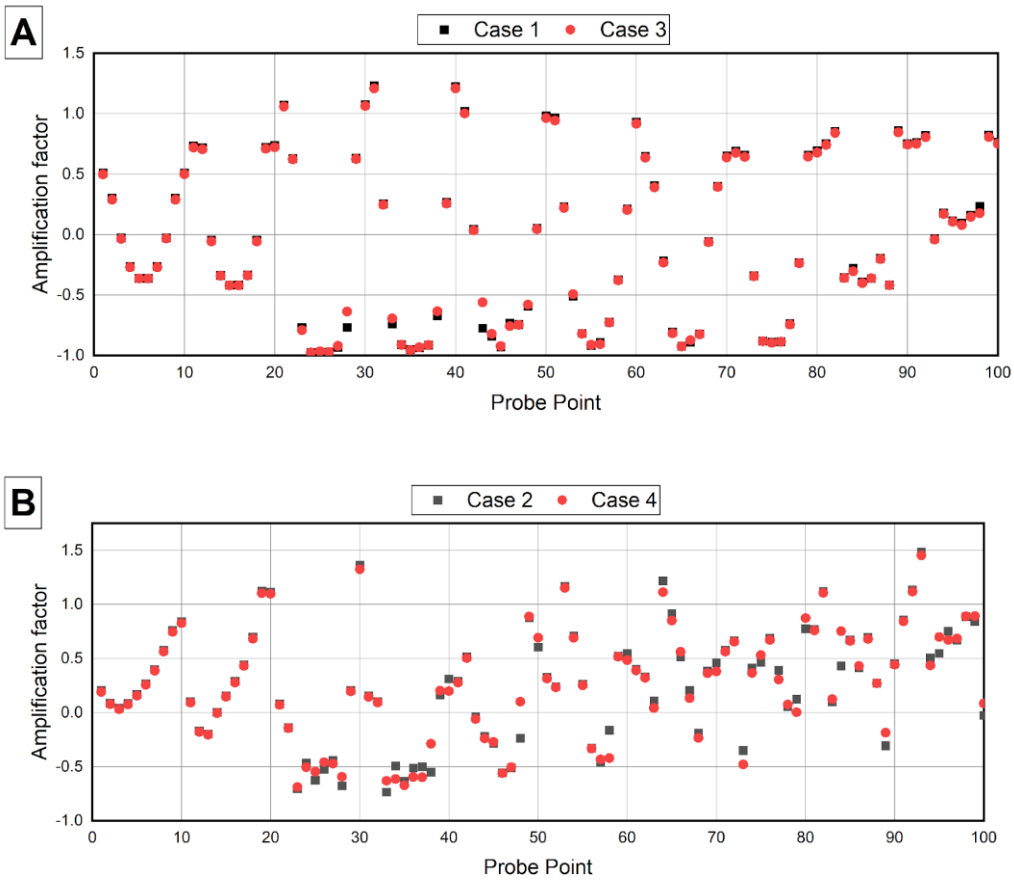

Figure 4-8. Amplification factor of the reference model

4.3. Perforated building wind performance

This section will characterize two geometrical features of the perforated building aerodynamics. The first feature is the profile of the perforation which is square and circular. At the same time, this section focuses on highlighting the probable aerodynamic effect of the angle of perforation draft angle (α). Therefore, each of the perforation profiles constructed with two α =45° and α =55°. For each case, the reference model with similar wind conditions used as a benchmark. Provided perforation expected to allow infiltration into the building and this phenomenon expected to increase the wind speed variable at the probe points inside the building. The admittance of the upstream wind into the building through the perforation may lead to pressure decline on the windward face of the building from the reference model.

4.3.1. Square perforation

Figure 4-9 and Figure 4-10 shows the distribution of velocity magnitude of the perforated building model. Figure 4-9 has a building perforation with a draft angle of 45° whereas Figure 4-10 model has a draft angle of 55°. From the image, a pressure buildup observed on the upstream side of the building as observed in the reference cases. However, the quantity of the pressure shows a 1% decline from the reference value. Also, there is a higher wind speed at the building edges, where there are significant wind jets. However, due to the air admitted to the building through the perforation holes, the U_{max} declined by 0.2m/s on average than the reference value. The color mapped result portrays a similar Figure 4-9 that cannot be distinct through visual inspection indicating the significant similarity in wind parameter result between the two draft angles. To help make a distinct numerical assessment of the wind parameters between the different models, the U_{max} results from all models recorded at the probe points plotted with its respective benchmark values in Figure 4-11.

The superimposition of the values in the graph shown in Figure 4-11 and Figure 4-12, categorized based on case wind condition. Cases with similar inlet values of wind speed and wind direction plotted in the same graph regardless of the geometrical feature. In Figure 4-11 and Figure 4-12a cases with Uref of 6 m/s and $\theta = 0°$ included. Whereas Figure 4-11b hosts cases with Uref of 6m/s at a direction of $\theta = 45°$. Figure 4-11c includes wind cases with conditions of 8m/s speed and $\theta = 0°$. The final graph has cases with Uref of 6 m/s at an angle of attack of $\theta = 45°$. Looking at the graphs it is unexpected to see how the perforated model's U_{max} value at the probe points is significantly like the nonperforated baseline model. The plot shows that the only U_{max} variance occurs on the probe point inside the building, indicating the effect of infiltration.

To observe the wind speed variation between the reference model and the perforated building categories in Figure 4-12, the wind speed value obtained for the perforated case divided by the reference value at the corresponding probe point. This operation shows there is a 14% and 11.5% amplification effect on average for cases 5 and 9, respectively. For Figure 4-12b, the velocity difference, referencing case 2, calculated at 17.2% and 16% for cases 6 and 10, respectively. In the case of Figure 4-12c, the value calculated was 15.7% and 13% for cases 7 and 11, respectively, taking case 3 as reference. And finally, with the model set with 8m/s wind speed and direction of $\theta = 45°$, the speed difference calculated at 15.5% and 14.3% for cases 8 and 12, respectively. All perforated building cases have shown a slight increment in the U_{max} record at the corresponding probe point from the reference model. This increment attributed to the admittance of wind to the inner space of the building through the perforation. The other observation is that when the draft angle of perforation increased from 45° to 55° in all cases the result showed decrement. The difference in value is even smaller when the wind speed is at an angle.

(A)

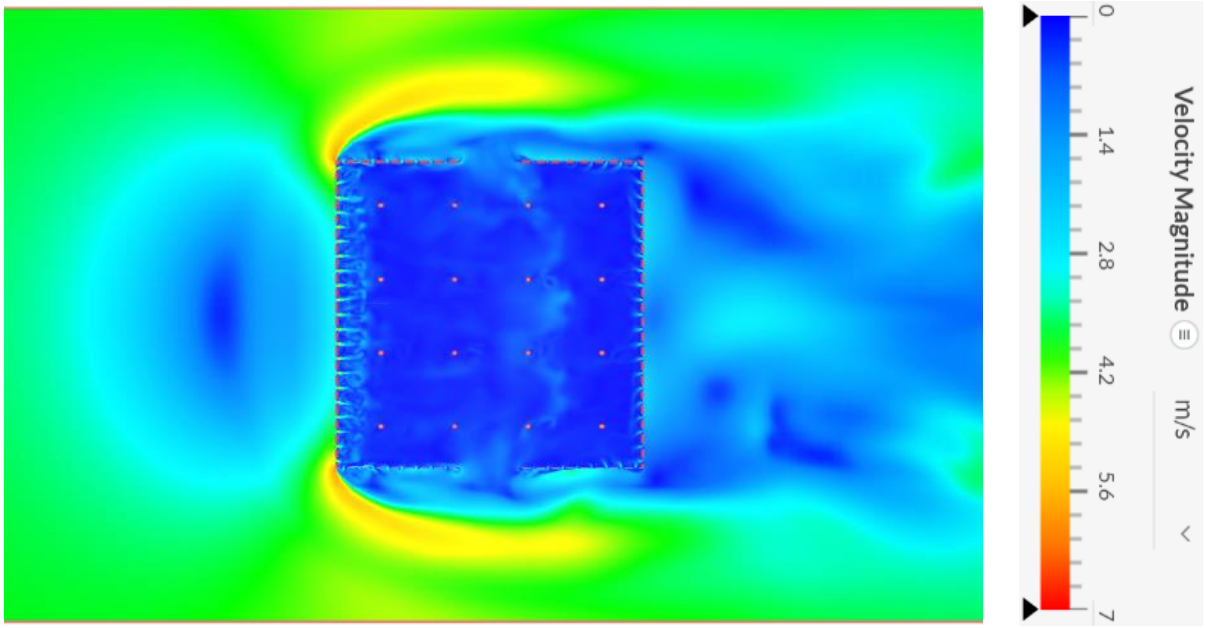

(B)

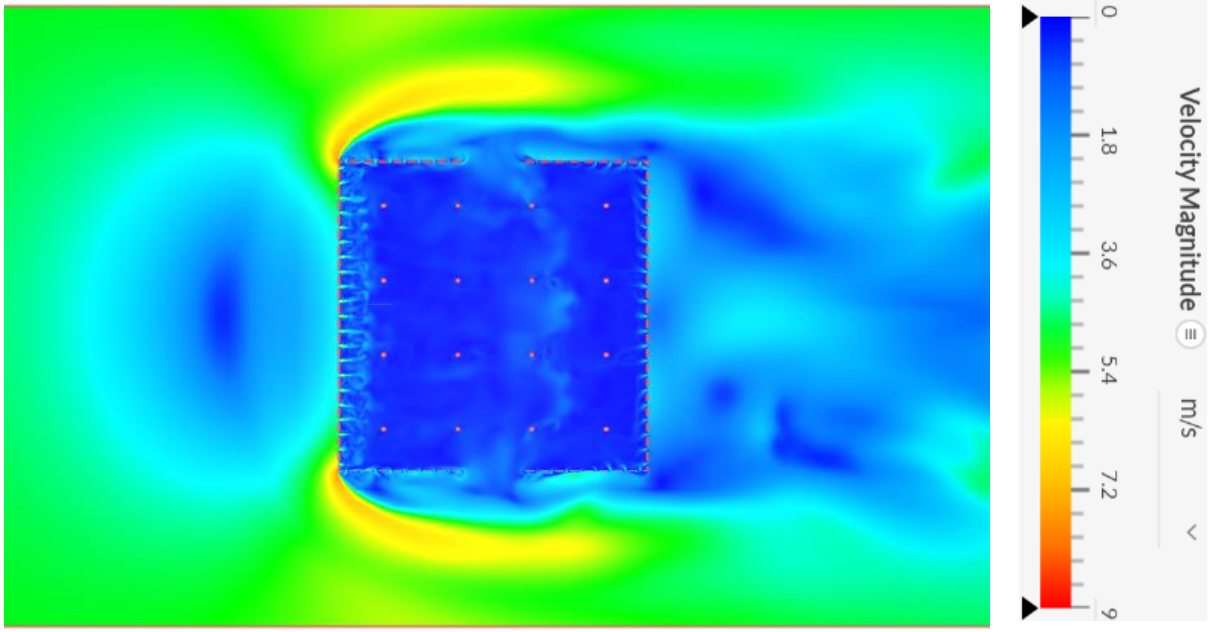

Figure 4-9. Color mapped average U_{mag} result of squire perforated building model at $\theta = 0°$ and wind reference velocity of (A) 6 m/s (B) 8 m/s

(A)

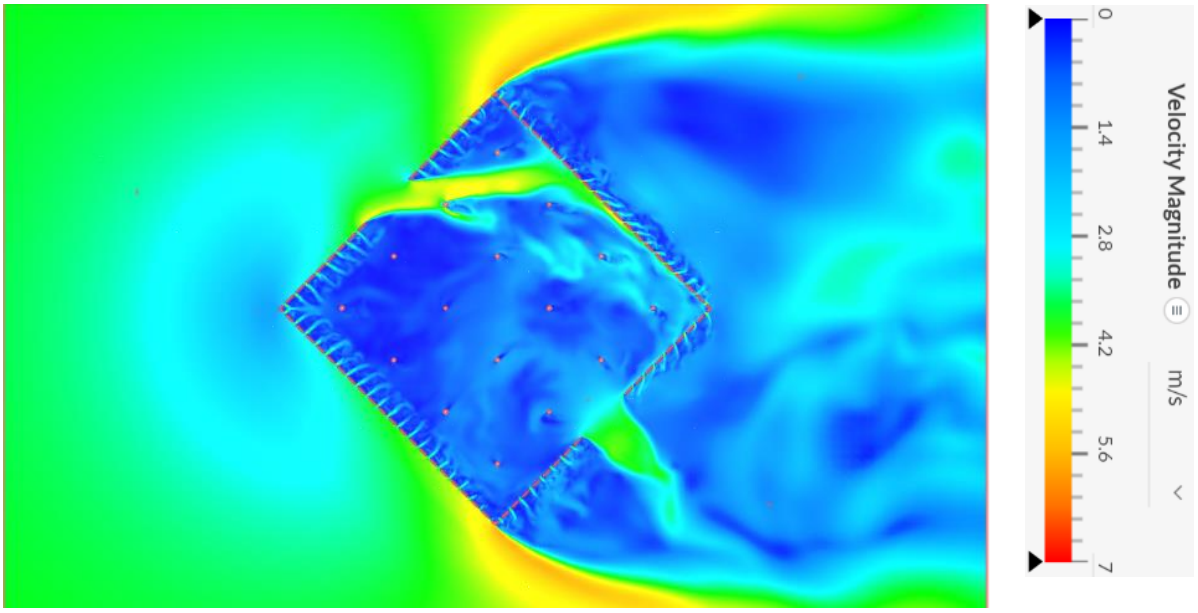

(B)

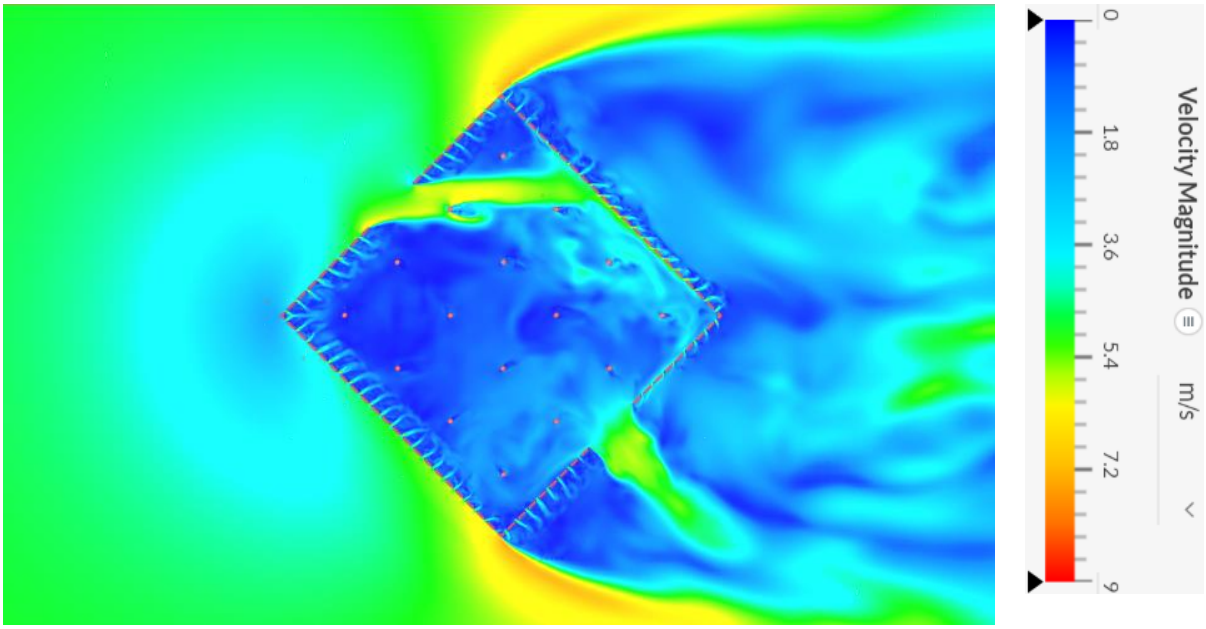

Figure 4-10. Color mapped average U_{mag} result of squire perforated building model at $\theta = 45°$ and wind reference velocity of (A) 6 m/s (B) 8 m/s

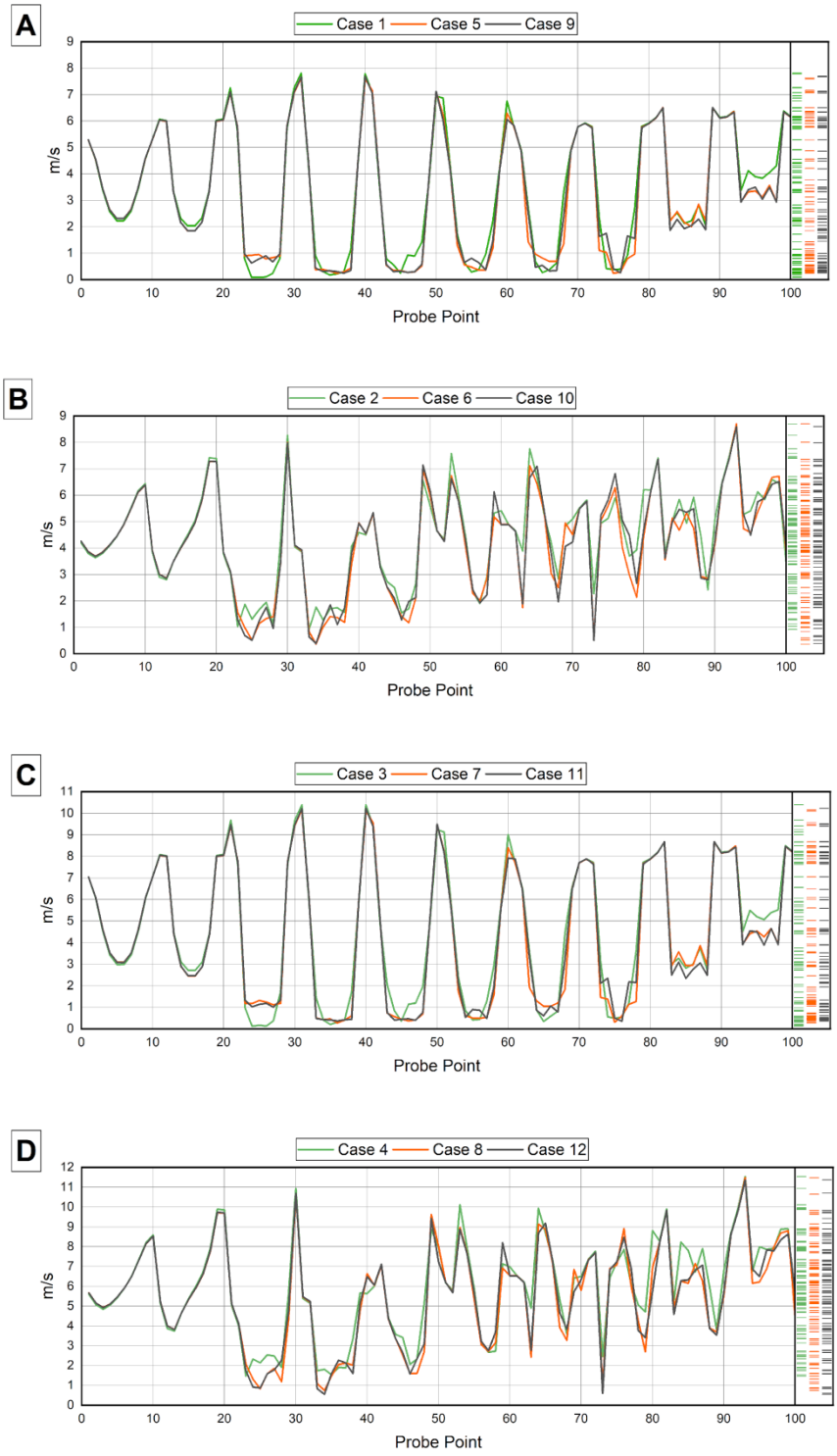

Figure 4-11. Comparison plot of squire perforated building models with the baseline model

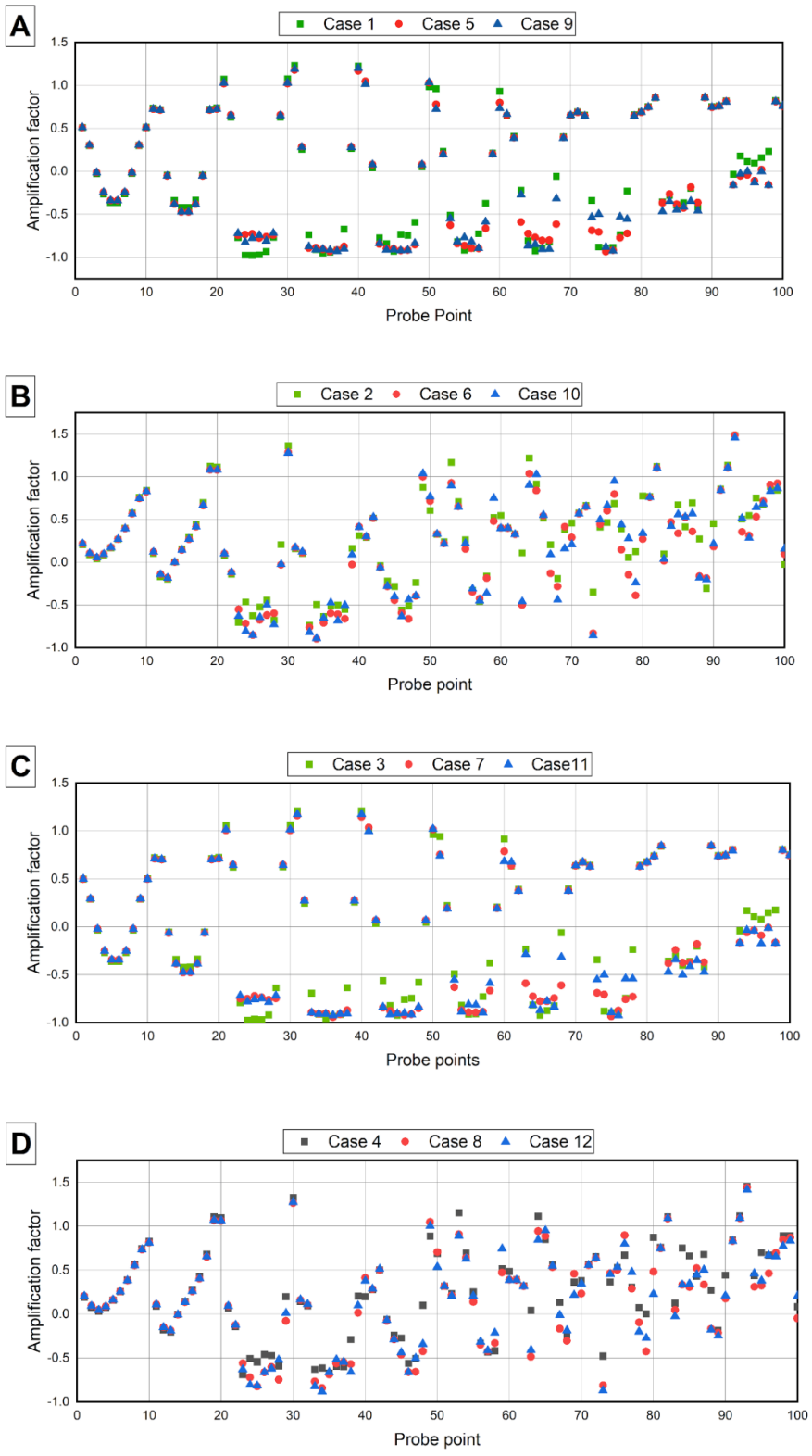

Figure 4-12. Amplification factor square perforated buildings corresponding with the baseline model

Figure 4-12 shows the amplification factor recorded at each probe point of the case sets where the values above the 0 mean amplification and below 0 is deceleration. When compared with the reference value, case 1, case 5 record equal amplification factors at 13 probe points and from which 2 measuring points are inside the building and the remaining located outside. Whereas case 9 shows a similar amplification with the reference case at 13 measuring points from which 2 positioned inside the building. Like the reference cases, cases 1 and 2, the perforated models, cases 6,5,91, and 10, recorded an amplification factor of over 1 at the measuring points 31, 40, 21, 30, 41, and 50. Since the study geometry is symmetrical, the result obtained at the probe point is equal to its symmetric correspondent and the points located at the upstream edge of the building. In the case of $\theta = 45°$ the measuring points, 93, 30, 64, 53, 92, 19,20, and 82, record a higher amplification factor of above 1. Unlike the cases with $\theta = 0°$, points that are inside the building in cases of $\theta = 45°$ show significant amplification effects.

4.3.2. Circular perforation wind performance

The impact of circular perforation geometry on wind amplification investigated based on the simulation in case set 3. Figure 4-13 and Figure 4-14 displayed the U_{mag} on a horizontal plane at a height of 2 meters above the ground (pedestrian height). Figure 4.13 have $\alpha = 45°$ and Figure 4.14 have $\alpha = 55°$ and all four cases presented in Figure 4-13 and Figure 4-14 have Uref of 6m/s. Similar observations to the previous cases can be made, in general, there is wind amplification at the upstream corner of the building and the perforation allows admittance of significant amounts of air in the building. Due to the perforation design with the draft, as the air passes through the perforation creates an air jet stream. In the case of $\alpha = 45°$, the air jet stream found to have a longer length than 55° cases.

The circular profile perforation cases show similarity in the recorded value of wind speed at the probe points in Figure 4-15. For cases with a wind condition of 6 m/s wind speed and with $\theta = 0°$ wind direction, Figure 4-15a, a value deviation from the reference model observed at probe points between 23 and 28. These points are located on the first row of probe points inside the building. The deviation recorded at this point is an increment in U_{max} indicating the influence of the air jet created by the perforation design. The second row of points inside the building, from 33 to 38, shows a decrement deviation from the reference value. This means the influence of the air jet is negligible at this distance far from the wall. The remaining array of measuring points in the 3rd, 4th, 5th, and 6th row has a similar velocity profile to the reference case. When the reference velocity increased to 8 m/s in Figure 4-15c, a similar velocity profile obtained with only amplitude increment due to the higher reference velocity. The result indicates that the amplification factor between the two case sets is close.

When the wind direction changes to $\theta = 45°$, the velocity profile is different from that of wind direction $\theta = 0°$. Despite the first two rows of measuring points recording a lower wind speed as shown in Figure 4-15b and d, the rest of the probe points inside the building show

significant wind speed increment from the corresponding model with θ = 0°. Even though a misalignment observed between the plotted values in Figure 4-15b, both perforated designs recorded a similar mean value of 4.18m/s showing a 0.2m/s smaller value from the corresponding reference case. Similarly, the perforated model in Figure 4-15d, cases 16 and 18, have a similar mean value of 5.5m/s. Whereas the reference model, case 4, has a mean value of 5.9m/s.

(A)

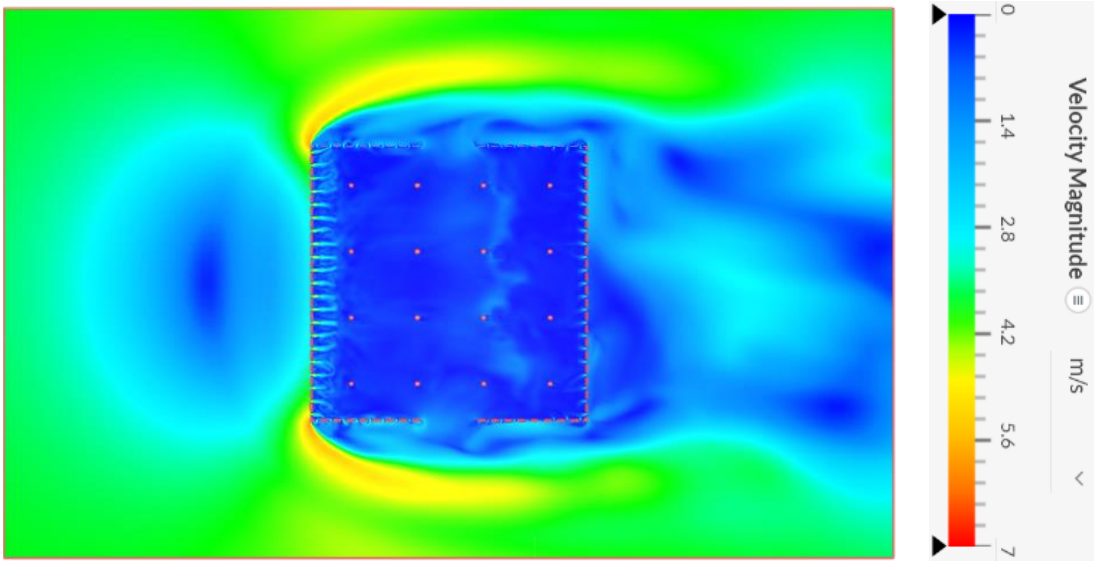

(B)

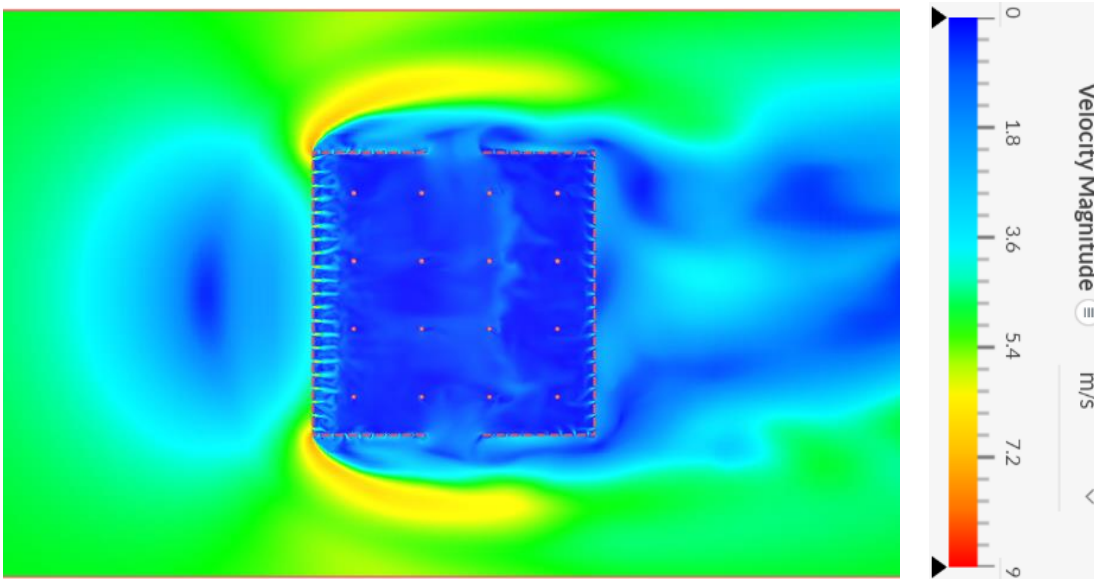

Figure 4-13. Color mapped average U_{mag} result of circular perforated building model at θ = 0° and wind reference velocity of (A) 6 m/s (B) 8 m/s

(A)

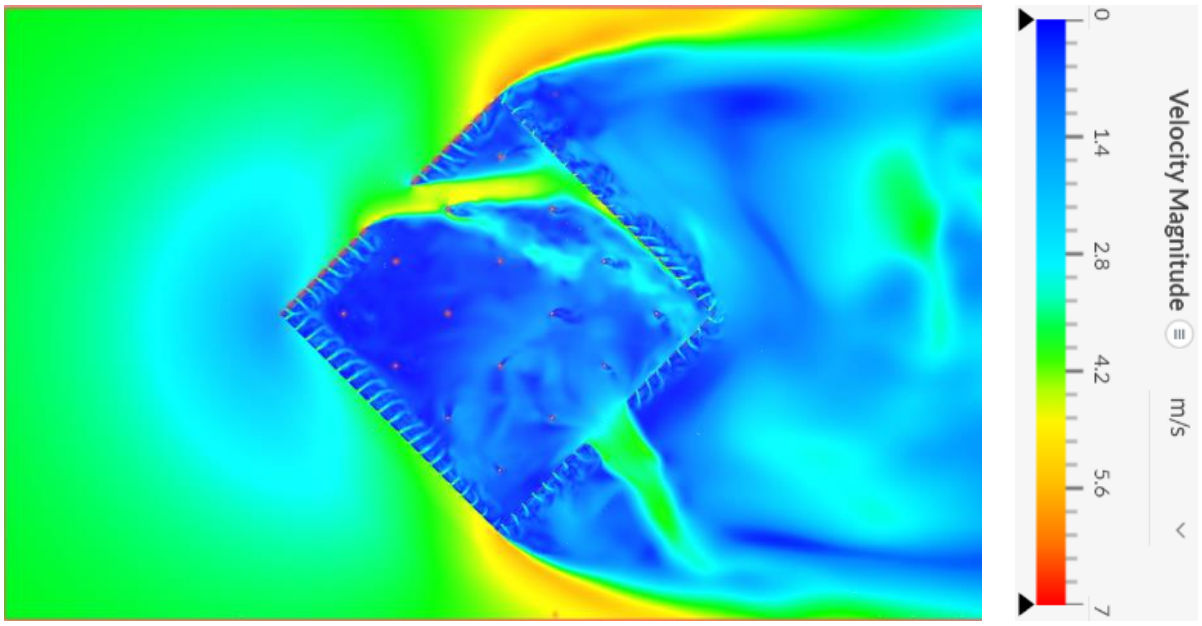

(B)

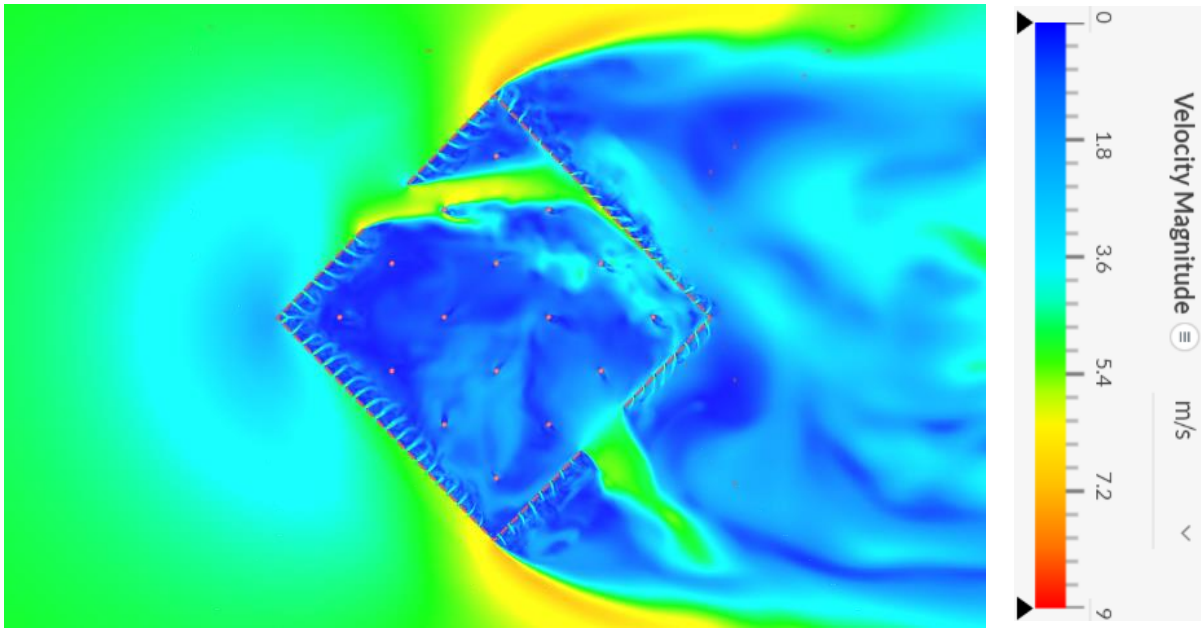

Figure 4-14. Color mapped average U_{mag} result of circular perforated building model at $\theta = 45°$ and wind reference velocity of (A) 6 m/s (B) 8 m/s

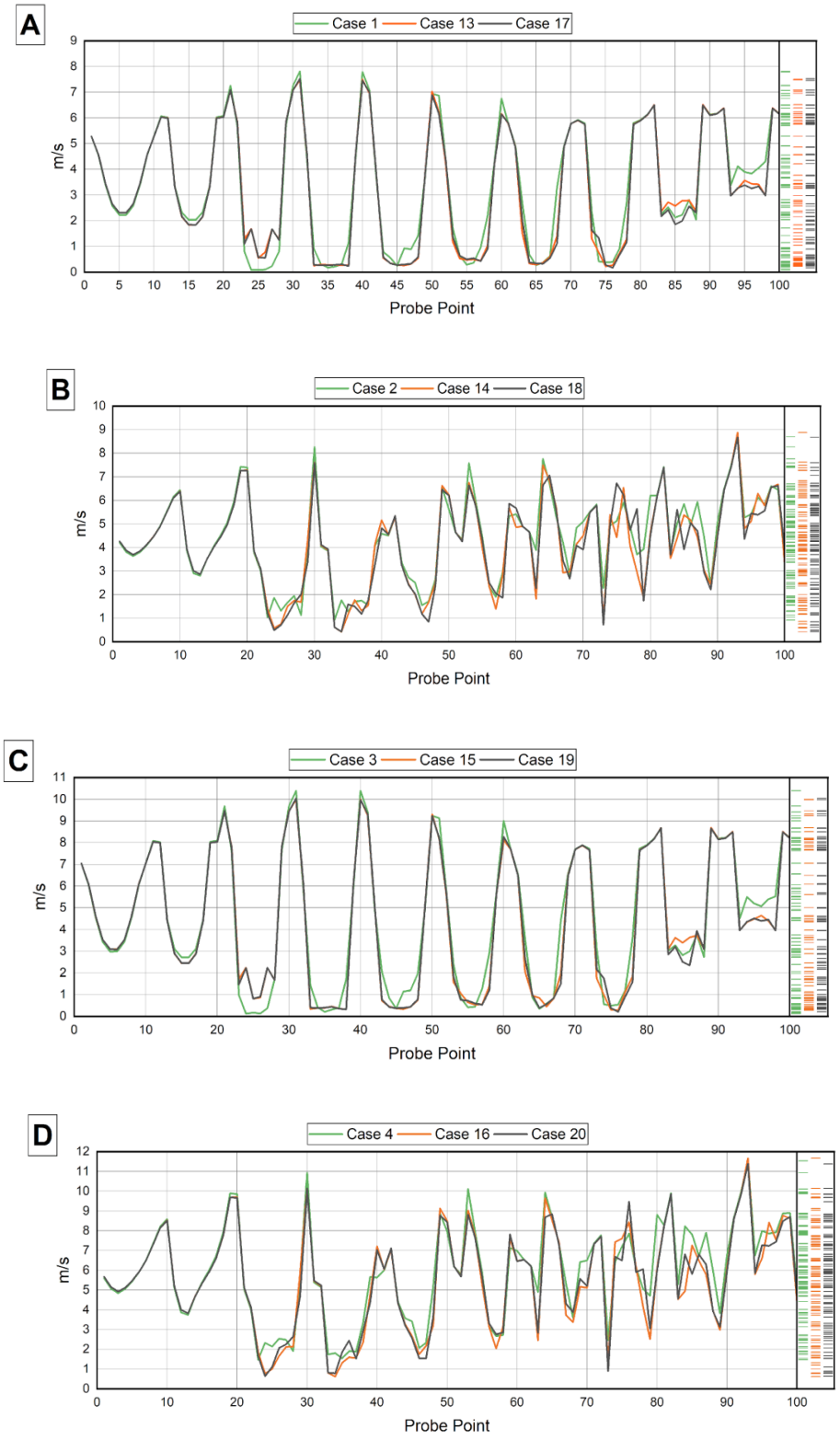

Figure 4-15. Comparison plot of circular perforated building model with the baseline models

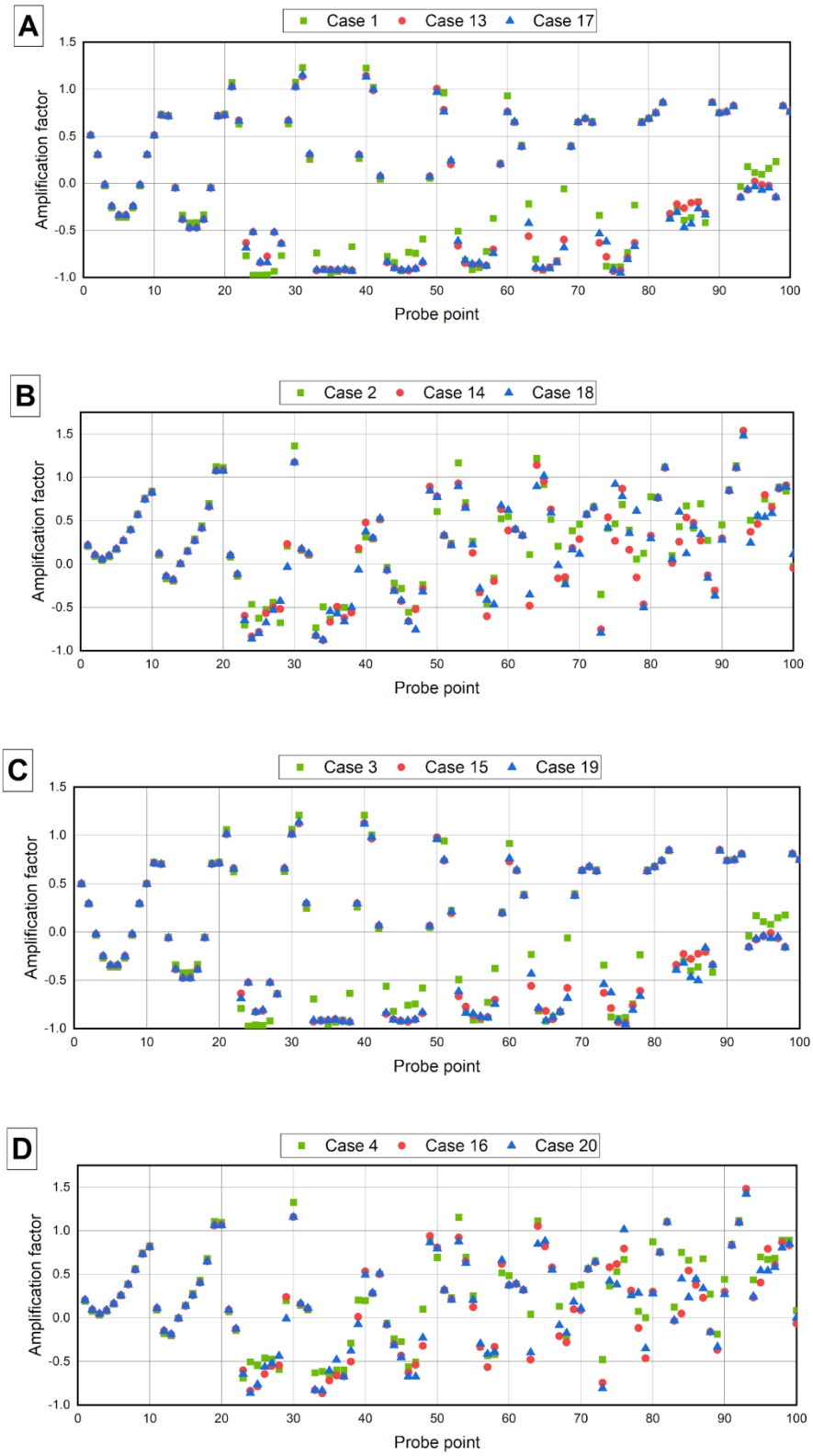

Figure 4-16. Amplification factor circular perforated building to corresponding reference model

In cases with θ = 45° a dispersed amplification factor observed as shown in Figure 4-16b and d when compared with the amplification factor of cases with θ = 0°, Figure 4-16a and c. Since similarity in mean U_{max} observed in Figure 4-16, we expected to obtain a similar wind amplification factor for perforated buildings with the same wind condition. Thus, the main interest is to observe amplification factor differences from the corresponding reference case. For Figure 4-16a, the mean amplification factor of the reference model, case 1, is -0.5 while the perforated models have a mean amplification factor of -0.8. In Figure 4-16a, the mean amplification factor of the reference case is 6% higher than perforated cases. In the third case set, Figure 4-16c, the reference case has a 4% higher mean amplification factor than the perforated cases. And finally, in the last set, the difference became 8% with the reference value recording a higher mean amplification factor.

4.4. Discussion

The previous section of the presented study used a reference study as a benchmark to evaluate results from the proposed case scenarios. This section of the study aims to discuss case models with results obtained from corresponding case scenarios. The study uses two geometrical characteristics (perforation geometry profile and perforation draft angle) and two wind conditions (wind speed and wind direction) to characterize the wind condition in the vicinity and inside of naturally ventilated buildings. The ventilation strategy follows a cross ventilation principle where the building faces designed with perforation to allow air to enter the building. To help investigate the phenomena 20 cases were prepared by combining both the geometrical and wind conditions as controlled variables to create investigation scenarios. The result from the case simulation from the early section combined into case groups based on their common features to conduct amplification factor trend analysis only in perforated models. Since the sequence of model set placement on the plot might influence the trend analysis, the study uses a simple placement sequence where square perforated buildings placed in the first half of the plot and circular perforated models follow.

4.4.1. Impact of wind condition

To discuss the influence of wind speed over the amplification factor, cases with similar geometrical features and wind direction but with different wind speeds grouped. Thus, one model set contains two cases with two different reference wind speeds (6 m/s and 8m/s). Like that of wind speed, to discuss wind speed increment caused due to wind direction change, cases with similar geometrical features and similar wind speed but different wind directions (θ = 0° and θ = 45°) grouped in a single model set. The reference geometrical model will not be included in this section as the section is interested in perforated models, resulting in eight pairs of models. After categorizing the model sets, the actual wind speed at the pedestrian height which is 3.5m/s for U_{ref} of 6m/s and 4.7m/s for wind reference speed of 8m/s subtracted from

U_{max} at each probe point of the case. The average value of this result plotted in Figure 4-17a and b for control variables of wind speed and wind direction, respectively.

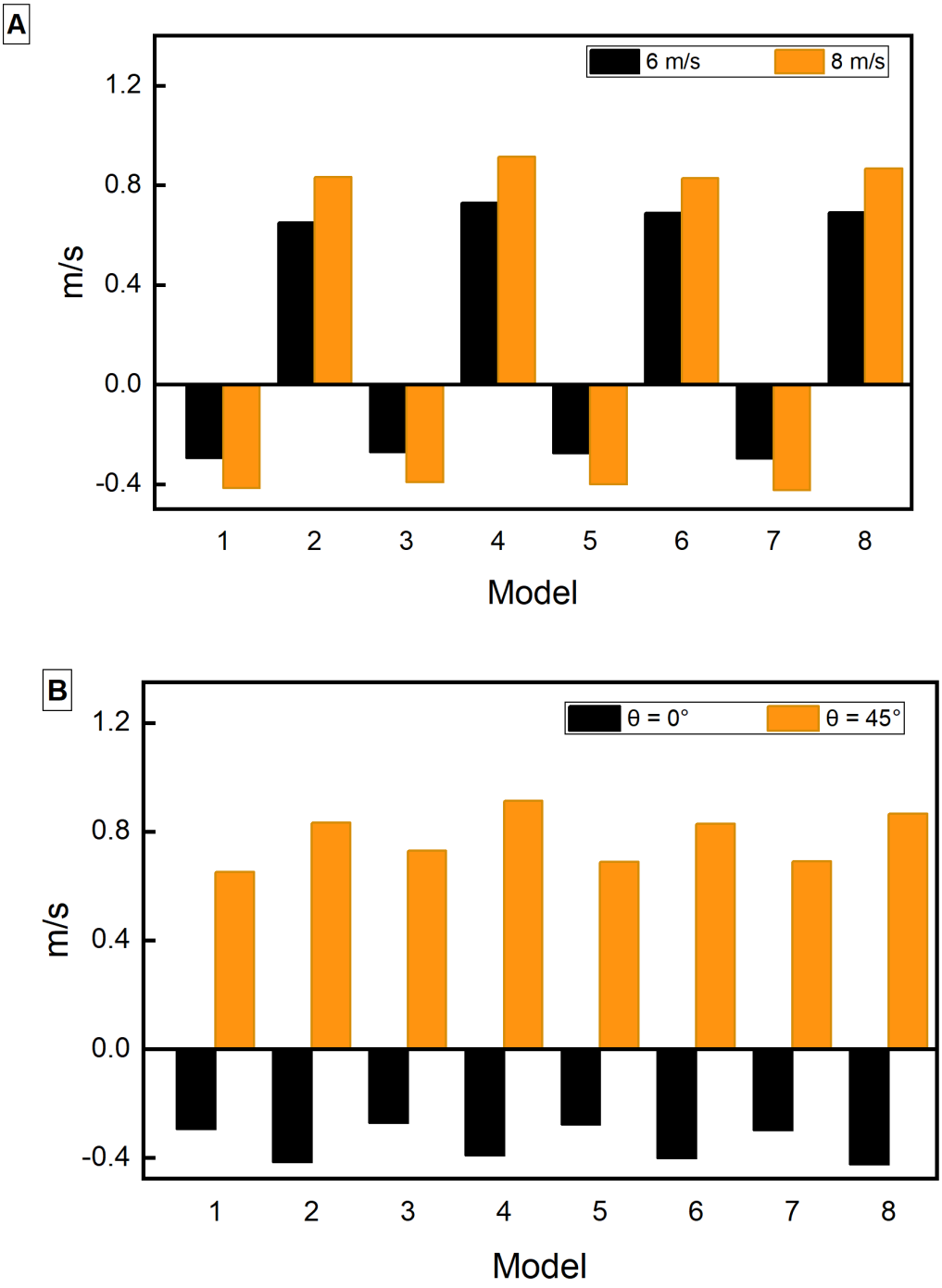

Figure 4-17. Impact of wind condition (A) group model with different wind speed (B) group model with different wind direction

For reference, in the case of perforated buildings with a square profile at a draft angle of 45° with the lower, case 5, and higher, case 7, reference values the difference calculated to be -

0.3m/s and -0.4m/s, respectively. In cases with square perforation design at 55° draft angle in cases 9 and 11, the difference calculated as -0.28m/s and -0.39m/s, respectively. For the circular building perforation, in the first two models with similar geometrical profiles, cases 13 and 15, the difference from the reference value calculated -0.28m/s and -0.4m/s, respectively. Finally, the two cases with similar geometrical features are cases 17 and 19 and their respective wind speed difference from the reference value is -0.3m/s and -0.42 m/s. For cases with θ=45°, a similar operation conducted, clustering cases with similar geometrical features, and the result of both cases presented in Figure 4-17a.

In Figure 4-17a, the measuring points record a wind speed value that is lower than the inflow wind speed for cases with a wind direction of θ = 0°. Whereas in the case of wind direction θ=45°, a significant wind increment from inflow wind speed is the result of the presence of the door opening upstream. As the reference inflow wind speed increased from 6m/s to 8 m/s, a significantly lower wind speed recorded at the measuring point in the case of θ = 0° shows an inverse relation. However, the relation is inverse for the cases with a wind direction of θ = 45°. The impact of wind direction in the proposed case models is distinct and clear having only one relation where θ=45° has a higher amplification effect as shown in Figure 4-17b.

4.4.2. Impact of building geometrical features

Two geometrical features of perforated building models featured in this study to investigate their effect on the local wind condition. These geometrical features are the geometrical profile of the perforation hole (square and circular) and the draft angle of the perforation (45° and 55°). To discuss the result here is the same procedure used as in the previous case, however, geometrical features become the control parameter. The resulting plot provided in Figure 4-18. To investigate the impact of the perforation profile on wind amplification, cases with similar wind condition and similar perforation draft angle, case 5 and 13, 6 and 14, 7 and 15, 8 and 16, 9 and 1, 10 and 18, 11 and 19, 12 and 20, paired in subsequent model sets as shown in Figure 4-18a.

From Figure 4-18 models set with θ = 45° have an amplification effect whereas models with θ = 0° have a deceleration factor of wind speed. In the first two model sets with a wind direction of θ = 45° and perforation draft angle of 45, model set 2 and 4, in Figure 4-18a, the case with a circular profile shows a slightly higher amplification effect than the square model. Whereas, in the last two models with a wind direction of θ=45° and perforation draft angle of 55°, the squire geometrical profile recorded a higher amplification effect. Cases with a wind direction of θ= 0° where the squire profile records a slightly higher deceleration factor with α = 45° and the circular profile required a higher deceleration factor for cases with α=55°. Figure 4-18b illustrates the relation between the two draft angles where the remaining study parameters remain the same. In the plot model, the result above the neutral line has a wind direction of θ = 45°, and the plotted result below the neutral line modeled with θ = 0°. In the plot above the

neutral line, α = 55° records a higher amplification effect when compared with α = 45°. However, the case of models under the neutral line has an inverse relation. And models with squire cases and α = 45° recorded a slightly higher acceleration factor. Model sets with circular profiles and α = 55° recorded a higher dissertation effect.

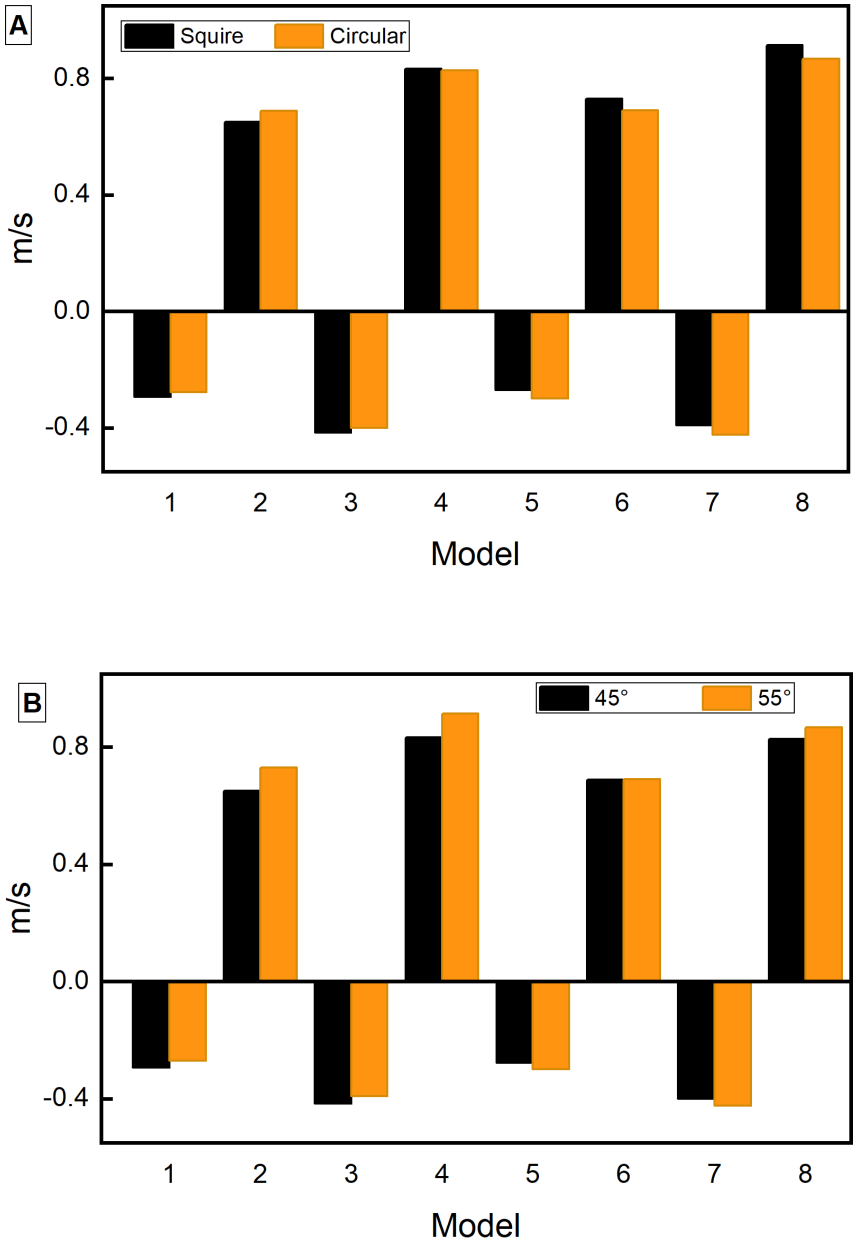

Figure 4-18. Impact of geometrical features (A) group model with different perforation deign (B) group model with different perforation draft angle

5. Conclusion and Recommendation

5.1. Conclusion

This study has performed a systematic sensitivity analysis based on different parameters and CFD simulation. In this study, the impact of geometrical characteristics and wind conditions of perforated buildings at pedestrian level wind conditions for naturally cross-ventilated buildings investigated. The lattice Boltzmann method used with a detached eddy version of the K-omega-SST turbulence model to perform a transient simulation. To record pedestrian level wind speed over the transient time over a hundred measuring points, 36 inside the building and 64 outside of the building, employed. To calculate the amplification effect of both geometrical features and wind condition of the proposed scenarios the maximum wind speed recorded at each probe point over the transient simulation selected as a target parameter. Thus, within the range of controlled parameters evaluated in the current study, we can conclude that the presence of perforation on buildings can reduce the pressure buildup on the upstream wall of the building through infiltration. With the infiltration occurring in this study, perforation geometrical characteristics such as the shape of the perforation and its design have a potential impact on wind conditions at a pedestrian height level in both indoor and outdoor wind environments. A significant flow change observed following the wind direction change inside the building recording high amplification factors. Hence, when buildings designed with perforation it is essential to consider the mechanical effect of wind inside the building.

5.2. Recommendation

For further studies, the study recommends characterizing activities inside cross-ventilated buildings to incorporate the impact in the comfort criteria and wind comfort analysis. To achieve that, the following limitation of the current study identified for further studies. First, this study only conducted for single perforation ratio, single envelope thickness, two inflow wind speeds, two wind directions, and four geometrical profiles. To extrude a dependable relation within the parameter, it is essential to increase the number of parameters and combinations. And lastly, the study focuses on an isolated building with perforations. In an actual urban environment, the aerodynamic interaction between buildings may lead to complexities of wind flow that result in different local wind conditions. Therefore, the likely interaction of a perforated cross-ventilated building with its surrounding building requires an investigation.

BIBLIOGRAPHY

Aghamolaei, R., Fallahpour, M., & Mirzaei, P. A. (2021). Tempo-spatial thermal comfort analysis of urban heat island with coupling of CFD and building energy simulation. *Energy and Buildings*, *251*, 111317.

Ai, Z. T., & Mak, C. M. (2015). From street canyon microclimate to indoor environmental quality in naturally ventilated urban buildings: Issues and possibilities for improvement. *Building and Environment*, *94*, 489–503.

Amorim, J. H., Valente, J., Pimentel, C., Freitas, S., Miranda, A. I., & Borrego, C. (2014). CFD modelling of the pedestrian wind comfort in a city avenue. *Aug*, *27*, 1–6.

Ampatzidis, P., & Kershaw, T. (2020). A review of the impact of blue space on the urban microclimate. *Science of The Total Environment*, *730*, 139068.

Bastide, A., Allard, F., & Boyer, H. (2007). Natural ventilation-A new method based on the Walton model applied to cross-ventilated buildings having two large external openings. *International Journal of Ventilation*, *6*(3), 195–206.

Beranek, W. J., & van Koten, H. (1979). Visual techniques for the determination of wind environment. *Journal of Wind Engineering and Industrial Aerodynamics*, *4*(3), 295–306. https://doi.org/10.1016/0167-6105(79)90009-6

Bherwani, H., Singh, A., & Kumar, R. (2020). Assessment methods of urban microclimate and its parameters: A critical review to take the research from lab to land. *Urban Climate*, *34*, 100690.

Birol, F. (2018). The future of cooling: Opportunities for energy-efficient air conditioning. *International Energy Agency*.

Blocken, B. (2014). 50 years of Computational Wind Engineering: Past, present and future. *Journal of Wind Engineering and Industrial Aerodynamics*, *129*, 69–102. https://doi.org/10.1016/j.jweia.2014.03.008

Blocken, B. (2015). Computational Fluid Dynamics for urban physics: Importance, scales, possibilities, limitations and ten tips and tricks towards accurate and reliable simulations. *Building and Environment*, *91*, 219–245. https://doi.org/10.1016/j.buildenv.2015.02.015

Blocken, B., & Gualtieri, C. (2012). Ten iterative steps for model development and evaluation applied to Computational Fluid Dynamics for Environmental Fluid Mechanics. *Environmental Modelling & Software*, *33*, 1–22. https://doi.org/10.1016/j.envsoft.2012.02.001

Blocken, B., Janssen, W. D., & van Hooff, T. (2012a). CFD simulation for pedestrian wind comfort and wind safety in urban areas: General decision framework and case study for the Eindhoven University campus. *Environmental Modelling & Software*, *30*, 15–34. https://doi.org/10.1016/j.envsoft.2011.11.009

Blocken, B., Janssen, W. D., & van Hooff, T. (2012b). CFD simulation for pedestrian wind comfort and wind safety in urban areas: General decision framework and case study for the Eindhoven University campus. *Environmental Modelling & Software*, *30*, 15–34. https://doi.org/10.1016/j.envsoft.2011.11.009

Blocken, B., Moonen, P., Stathopoulos, T., & Carmeliet, J. (2008). Numerical study on the existence of the venturi effect in passages between perpendicular buildings. *Journal of Engineering Mechanics*, *134*(12), 1021–1028.

Blocken, B., & Persoon, J. (2009). Pedestrian wind comfort around a large football stadium in an urban environment: CFD simulation, validation and application of the new Dutch wind nuisance standard. *Journal of Wind Engineering and Industrial Aerodynamics*, *97*(5–6), 255–270.

Blocken, B., Stathopoulos, T., & Carmeliet, J. (2007). CFD simulation of the atmospheric boundary layer: Wall function problems. *Atmospheric Environment*, *41*(2), 238–252.

Blocken, B., Stathopoulos, T., & Carmeliet, J. (2008). Wind Environmental Conditions in Passages between Two Long Narrow Perpendicular Buildings. *Journal of Aerospace Engineering*, *21*(4), 280–287. https://doi.org/10.1061/(ASCE)0893-1321(2008)21:4(280)

Brager, G., & de Dear, R. (2000). *A standard for natural ventilation*.

Causone, F. (2016). Climatic potential for natural ventilation. *Architectural Science Review*, *59*(3), 212–228.

Chen, Y., Tong, Z., & Malkawi, A. (2017). Investigating natural ventilation potentials across the globe: Regional and climatic variations. *Building and Environment*, *122*, 386–396.

Conan, B., van Beeck, J., & Aubrun, S. (2012). Sand erosion technique applied to wind resource assessment. *Journal of Wind Engineering and Industrial Aerodynamics*, *104–106*, 322–329. https://doi.org/10.1016/j.jweia.2012.03.017

Dissanayaka, C. (2021). URBAN VEGETATION AND MORPHOLOGY PARAMETERS AFFECTING MICROCLIMATE AND OUTDOOR THERMAL COMFORT IN WARM HUMID CITIES–A REVIEW OF RESEARCH IN THE PAST DECADE. *Proceedings of The International Conference on Climate Change*, *5*(1), 1–17.

Durgin, F. H. (1992). Pedestrian level wind studies at the Wright brothers facility. *Journal of Wind Engineering and Industrial Aerodynamics*, *44*(1), 2253–2264. https://doi.org/10.1016/0167-6105(92)90016-4

Franke, J., Hellsten, A., Schlünzen, K. H., & Carissimo, B. (2007). Best practice guideline for the CFD simulation of flows in the urban environment—A summary. *11th Conference on Harmonisation within Atmospheric Dispersion Modelling for Regulatory Purposes, Cambridge, UK, July 2007*. https://research.aalto.fi/en/publications/best-practice-guideline-for-the-cfd-simulation-of-flows-in-the-ur

Gago, E. J., Roldan, J., Pacheco-Torres, R., & Ordóñez, J. (2013). The city and urban heat islands: A review of strategies to mitigate adverse effects. *Renewable and Sustainable Energy Reviews*, *25*, 749–758. https://doi.org/10.1016/j.rser.2013.05.057

Hami, A., Abdi, B., Zarehaghi, D., & Maulan, S. B. (2019). Assessing the thermal comfort effects of green spaces: A systematic review of methods, parameters, and plants' attributes. *Sustainable Cities and Society*, *49*, 101634. https://doi.org/10.1016/j.scs.2019.101634

Ijeoma, N. (2021, October 11). Africa's iconic architecture in 12 buildings. *BBC News*. https://www.bbc.com/news/world-africa-58855205

Irwin, H. P. A. H. (1981). A simple omnidirectional sensor for wind-tunnel studies of pedestrian-level winds. *Journal of Wind Engineering and Industrial Aerodynamics*, *7*(3), 219–239. https://doi.org/10.1016/0167-6105(81)90051-9

Isyumov, N., & Davenport, A. G. (1975). Comparison of full-scale and wind tunnel wind speed measurements in the commerce court plaza. *Journal of Wind Engineering and Industrial Aerodynamics*, *1*, 201–212. https://doi.org/10.1016/0167-6105(75)90014-8

Jamieson, N. J., Carpenter, P., & Cenek, P. D. (1992). The effect of architectural detailing on pedestrian level wind speeds. *Journal of Wind Engineering and Industrial Aerodynamics*, *44*(1), 2301–2312. https://doi.org/10.1016/0167-6105(92)90020-B

Janssen, W. D., Blocken, B., & van Hooff, T. (2013). Pedestrian wind comfort around buildings: Comparison of wind comfort criteria based on whole-flow field data for a complex case study. *Building and Environment*, *59*, 547–562.

Jiang, Y., & Chen, Q. (2002). Effect of fluctuating wind direction on cross natural ventilation in buildings from large eddy simulation. *Building and Environment*, *37*(4), 379–386.

Kamei, I., & Maruta, E. (1979). Study on wind environmental problems caused around buildings in Japan. *Journal of Wind Engineering and Industrial Aerodynamics*, *4*(3), 307–331. https://doi.org/10.1016/0167-6105(79)90010-2

Kawamura, S., Kimoto, E., Fukushima, T., & Taniike, Y. (1988). Environmental wind characteristics around the base of a tall building—A comparison between model test and full scale experiment -. *Journal of Wind Engineering and Industrial Aerodynamics*, *28*(1), 149–158. https://doi.org/10.1016/0167-6105(88)90111-0

Lam, K. M. (1992). Wind environment around the base of a tall building with a permeable intermediate floor. *Journal of Wind Engineering and Industrial Aerodynamics*, *44*(1), 2313–2314. https://doi.org/10.1016/0167-6105(92)90021-2

Lenzholzer, S., & Brown, R. D. (2016). Post-positivist microclimatic urban design research: A review. *Landscape and Urban Planning*, *153*, 111–121.

Livesey, F., Inculet, D., Isyumov, N., & Davenport, A. G. (1990). A scour technique for the evaluation of pedestrian winds. *Journal of Wind Engineering and Industrial Aerodynamics*, *36*, 779–789. https://doi.org/10.1016/0167-6105(90)90075-N

Livesey, F., Morrish, D., Mikitiuk, M., & Isyumov, N. (1992). Enhanced scour tests to evaluate pedestrian level winds. *Journal of Wind Engineering and Industrial Aerodynamics*, *44*(1), 2265–2276. https://doi.org/10.1016/0167-6105(92)90017-5

Mei, R., Shyy, W., Yu, D., & Luo, L.-S. (2000). Lattice Boltzmann Method for 3-D Flows with Curved Boundary. *Journal of Computational Physics*, *161*(2), 680–699. https://doi.org/10.1006/jcph.2000.6522

Motazedian, A., & Leardini, P. (2012). *Impact of green infrastructures on urban microclimates: A critical review of data collection methods*.

Murakami, S., Uehara, K., & Komine, H. (1979). Amplification of wind speed at ground level due to construction of high-rise building in urban area. *Journal of Wind Engineering and Industrial Aerodynamics*, *4*(3), 343–370. https://doi.org/10.1016/0167-6105(79)90012-6

Pool, D. A. C. (2019). A Comprehensive Evaluation of Perforated Façades for Daylighting and Solar Shading Performance: Effects of Matrix, Thickness and Separation Distance. *Journal of Daylighting*, *6*(2), 97–111. https://doi.org/10.15627/jd.2019.10

Priya, U. K., & Senthil, R. (2021). A review of the impact of the green landscape interventions on the urban microclimate of tropical areas. *Building and Environment*, *205*, 108190.

Programme, U. N. E. (2020). *2020 Global Status Report for Buildings and Construction: Towards a Zero-Emission, Efficient and Resilient Buildings and Construction Sector*. United Nations Environment Programme Nairobi, Kenya.

Qian, Y. H., D'Humières, D., & Lallemand, P. (1992). Lattice BGK Models for Navier-Stokes Equation. *Europhysics Letters (EPL)*, *17*(6), 479–484. https://doi.org/10.1209/0295-5075/17/6/001

Raja, I. A., Nicol, J. F., McCartney, K. J., & Humphreys, M. A. (2001). Thermal comfort: Use of controls in naturally ventilated buildings. *Energy and Buildings*, *33*(3), 235–244.

Ratcliff, M. A., & Peterka, J. A. (1990). Comparison of pedestrian wind acceptability criteria. *Journal of Wind Engineering and Industrial Aerodynamics*, *36*, 791–800.

Reiter, S. (2010). Assessing Wind Comfort in Urban Planning: *Environment and Planning B: Planning and Design*. https://doi.org/10.1068/b35154

Ricci, A., Guasco, M., Caboni, F., Orlanno, M., Giachetta, A., & Repetto, M. P. (2022). Impact of surrounding environments and vegetation on wind comfort assessment of a new tower with vertical green park. *Building and Environment*, *207*, 108409.

rodforctgov.com. (n.d.). RODFORCT | Natural ventilation control. *NATURAL VENTILATION CONTROL*. Retrieved June 2, 2022, from https://rodforctgov.com/real-estate/natural-ventilation-control/

Rodriguez-Ubinas, E., Montero, C., Porteros, M., Vega, S., Navarro, I., Castillo-Cagigal, M., Matallanas, E., & Gutiérrez, A. (2014). Passive design strategies and performance of Net Energy Plus Houses. *Energy and Buildings*, *83*, 10–22.

Sandberg, M. (2004). An alternative view on the theory of cross-ventilation. *International Journal of Ventilation*, *2*(4), 409–418.

Sasaki, R., Uematsu, Y., Yamada, M., & Saeki, H. (1997). Application of infrared thermography and a knowledge-based system to the evaluation of the pedestrian-level wind environment around buildings. *Journal of Wind Engineering and Industrial Aerodynamics*, *67–68*, 873–883. https://doi.org/10.1016/S0167-6105(97)00125-6

Schinasi, L. H., Benmarhnia, T., & De Roos, A. J. (2018). Modification of the association between high ambient temperature and health by urban microclimate indicators: A systematic review and meta-analysis. *Environmental Research*, *161*, 168–180.

SimScale, G. (2022). *Incompressible Lattice Boltzmann Method | Advanced*. SimScale. https://www.simscale.com/docs/incompressible-lbm-lattice-boltzmann-advanced/

Sinha, N. (2013). Towards RANS Parameterization of Vertical Mixing by Langmuir Turbulence in Shallow Coastal Shelves. *Graduate Theses and Dissertations*. https://digitalcommons.usf.edu/etd/4945

Stathopoulos, T. (1985). Wind environmental conditions around tall buildings with chamfered corners. *Journal of Wind Engineering and Industrial Aerodynamics*, *21*(1), 71–87. https://doi.org/10.1016/0167-6105(85)90034-0

Stavrakakis, G. M., Koukou, M. K., Vrachopoulos, M. G., & Markatos, N. C. (2008). Natural cross-ventilation in buildings: Building-scale experiments, numerical simulation and thermal comfort evaluation. *Energy and Buildings*, *40*(9), 1666–1681.

Taheri, J., Moghadam, T. T., Taheri, S., Safari, M. K., & Eslami, F. (2021). Assessment of passive design strategies in traditional houses of Sabzevar, Iran. *Journal of Cultural Heritage Management and Sustainable Development*.

Tominaga, Y., Mochida, A., Yoshie, R., Kataoka, H., Nozu, T., Yoshikawa, M., & Shirasawa, T. (2008). AIJ guidelines for practical applications of CFD to pedestrian wind environment around buildings. *Journal of Wind Engineering and Industrial Aerodynamics*, *96*(10–11), 1749–1761.

Tsoka, S., Tsikaloudaki, K., Theodosiou, T., & Bikas, D. (2020). Urban Warming and Cities' Microclimates: Investigation Methods and Mitigation Strategies—A Review. *Energies*, *13*(6), 1414.

United Nations, U. P. (2019). *World urbanization prospects :* UN,. https://digitallibrary.un.org/record/3833745

White, B. R. (1992). Analysis and wind-tunnel simulation of pedestrian-level winds in San Francisco. *Journal of Wind Engineering and Industrial Aerodynamics*, *44*(1), 2353–2364. https://doi.org/10.1016/0167-6105(92)90026-7

Willemsen, E., & Wisse, J. A. (2007a). Design for wind comfort in The Netherlands: Procedures, criteria and open research issues. *Journal of Wind Engineering and Industrial Aerodynamics*, *95*(9–11), 1541–1550.

Willemsen, E., & Wisse, J. A. (2007b). Design for wind comfort in The Netherlands: Procedures, criteria and open research issues. *Journal of Wind Engineering and Industrial Aerodynamics*, *95*(9), 1541–1550. https://doi.org/10.1016/j.jweia.2007.02.006

Williams, C. D., & Wardlaw, R. L. (1992). Determination of the pedestrian wind environment in the city of Ottawa using wind tunnel and field measurements. *Journal of Wind Engineering and Industrial Aerodynamics*, *41*(1), 255–266. https://doi.org/10.1016/0167-6105(92)90418-A

williams.com. (2018). *Passive Solar Design*. Sustainability. https://sustainability.williams.edu/green-building-basics/passive-solar-design/

Wu, H., & Stathopoulos, T. (1994). Further experiments on Irwin's surface wind sensor. *Journal of Wind Engineering and Industrial Aerodynamics*, *53*(3), 441–452. https://doi.org/10.1016/0167-6105(94)90095-7

Yamada, M., Uematsu, Y., & Sasaki, R. (1996). A visual technique for the evaluation of the pedestrian-level wind environment around buildings by using infrared thermography. *Journal of Wind Engineering and Industrial Aerodynamics*, *65*(1), 261–271. https://doi.org/10.1016/S0167-6105(97)00045-7

Yao, R., Costanzo, V., Li, X., Zhang, Q., & Li, B. (2018). The effect of passive measures on thermal comfort and energy conservation. A case study of the hot summer and cold winter climate in the Yangtze River region. *Journal of Building Engineering*, *15*, 298–310.

Yu, D., Mei, R., Luo, L.-S., & Shyy, W. (2003). Viscous flow computations with the method of lattice Boltzmann equation. *Progress in Aerospace Sciences*, *39*(5), 329–367.

Zhang, Y., Wang, J., Chen, H., Zhang, J., & Meng, Q. (2010). Thermal comfort in naturally ventilated buildings in hot-humid area of China. *Building and Environment*, *45*(11), 2562–2570.